

# The Statistical Properties of Neutral Gas at $z < 1.65$ from UV Measurements of Damped Lyman Alpha Systems<sup>★</sup>

Sandhya M. Rao,<sup>1†</sup> David A. Turnshek,<sup>1</sup> Gendith M. Sardane<sup>1</sup> and Eric M. Monier<sup>2</sup>

<sup>1</sup>*Department of Physics and Astronomy and PITTsburgh Particle physics, Astrophysics, and Cosmology Center (PITT PACC), University of Pittsburgh, Pittsburgh, PA 15260, USA*

<sup>2</sup>*Department of Physics, The College at Brockport, State University of New York, Brockport, NY 14420, USA*

Accepted XXX. Received YYY; in original form ZZZ

## ABSTRACT

We derive the statistical properties of neutral gas at redshifts  $0.11 < z < 1.65$  from UV measurements of quasar Ly $\alpha$  absorption lines corresponding to 369 Mg II systems with  $W_0^{42796} \geq 0.3$  Å. In addition to the 41 damped Lyman alpha (DLA) systems presented in Rao et al. (2006), the current DLA sample includes 29 newly discovered DLAs. Of these, 26 were found in our *Hubble Space Telescope* (HST) Advanced Camera for Surveys prism survey for DLAs (Turnshek et al. 2015) and three were found in a *GALaxy Evolution Explorer* (GALEX) archival search. In addition, an HST Cosmic Origins Spectrograph Cycle 19 survey yielded no DLAs that could be used for this study. Formally, this DLA sample includes 70 systems with  $N_{\text{HI}} \geq 2 \times 10^{20}$  atoms cm<sup>-2</sup>. We find that the incidence of DLAs, or the product of their gas cross section and their comoving number density, can be described by  $n_{\text{DLA}}(z) = (0.027 \pm 0.007)(1+z)^{(1.682 \pm 0.200)}$  over the redshift range  $0 < z < 5$ . The cosmic mass density of neutral gas can be described by  $\Omega_{\text{DLA}}(z) = (4.77 \pm 1.60) \times 10^{-4}(1+z)^{(0.64 \pm 0.27)}$ . The low-redshift column density distribution function is well-fitted by a power law of the form  $f(N) \sim N^\beta$  with  $\beta = -1.46 \pm 0.20$ . It is consistent with the high-redshift as well as  $z = 0$  estimates at the high column density end but, lies between them at the low column density end. We discuss possible  $N_{\text{HI}}$  and metallicity bias in Mg II-selected DLA samples and show that such biases do not exist in the current data at  $z < 1.65$ . Thus, at least at  $z < 1.65$ , DLAs found through Mg II selection statistically represent the true population of DLAs. However, we caution that studies of DLA metallicities should take into the account the relative incidence of DLAs with respect to  $W_0^{42796}$  (or gas velocity spread) in order to correctly measure the mean neutral-gas cosmic metallicity of the universe.

**Key words:** galaxies evolution - galaxies ISM - galaxies formation - quasars absorption lines

## 1 INTRODUCTION

For decades, quasar absorption line surveys have proved to be a powerful and highly successful way of probing intervening gaseous structures in the Universe. Studying the redshift evolution of absorption lines, be they lines of molecular H<sub>2</sub>, neutral H I, or metals, allows us to trace the star

formation and galaxy assembly history of the Universe without being biased by the luminous components of galaxies. In particular, the damped Lyman alpha (DLA) systems, which have the highest observed neutral hydrogen column densities,  $N_{\text{HI}} \geq 2 \times 10^{20}$  atoms cm<sup>-2</sup>, are known to contain the bulk of the neutral gas mass in the Universe (see Wolfe et al. 2005 for an overview of DLA research.) Since the original Lick survey for DLAs (Wolfe et al. 1986), many teams have advanced the field at redshifts  $z \geq 1.65$ , where the Ly $\alpha$  line falls in the optical part of the spectrum and can be accessed with ground-based telescopes (Turnshek et al. 1989; Lanzetta et al. 1991; Storrie-Lombardi & Wolfe 2000; Péroux et al. 2003; Prochaska & Herbert-Fort 2004; Prochaska, Herbert-Fort, & Wolfe 2005; Ellison et al. 2008;

<sup>★</sup> Based on data obtained from the Sloan Digital Sky Survey (SDSS) and on observations made with the *Hubble Space Telescope* (HST) operated by STScI-AURA for NASA/ESA and the NASA *Galaxy Evolution Explorer* (GALEX) operated for NASA by the California Institute of Technology under NASA contract NAS5-98034.

<sup>†</sup> E-mail srao@pitt.edu

Prochaska & Wolfe 2009; Noterdaeme et al. 2009; 2012; Zafar et al. 2013a; 2013b; Crighton et al. 2015; Sánchez-Ramírez et al. 2016). This was accomplished by measuring the properties of the DLAs and considering successively larger samples, which statistically improved the accuracy of the results on the DLA incidence and cosmic neutral gas mass density at  $z \geq 1.65$ . The number of known DLA systems at these higher redshifts increased from  $\sim 15$  in the Lick survey to over 6800 in the Sloan Digital Sky Survey III (Data Release 9) quasar spectroscopic database (Noterdaeme et al. 2012, henceforth, N12).

Nevertheless, DLAs are rare, especially at redshifts  $z < 1.65$  – an interval that includes the most recent  $\sim 70\%$  of the age of the Universe – where the line falls in the UV. The HST Quasar Absorption Line Key Project found only 1 DLA in a blind survey (Bahcall et al. 1993), while Meiring et al. (2011) found 3 serendipitous DLAs in the COS-Halos survey, and Neeleman et al. (2016) identified 4 DLAs in a blind survey of 463 quasars in the HST archives. These results are consistent given the small samples and low statistical accuracies. Thus, given the limited availability of space-based observing time for UV surveys, the identification of a substantial sample of ‘UV’-redshift DLAs in a blind spectroscopic survey is practically impossible, not to mention extremely inefficient. Therefore, to isolate sightlines which have DLAs, we used a technique that exploited the fact that all known optical-redshift DLAs have strong Mg II absorption, i.e., with Mg II  $\lambda 2796$  rest equivalent width  $W_0^{\lambda 2796} \geq 0.3$  Å, to construct a survey for DLAs in a sample of Mg II absorbers (Rao, Turnshek, & Briggs 1995; Rao & Turnshek 2000; Rao, Turnshek, & Nestor 2006, henceforth RTN06). We emphasize here that the strong-Mg II-selection method is primarily a selection based on gas velocity spread since Mg II absorption lines are generally saturated. Therefore, the lines become strong when their velocity spread (or number of components) is large, and not because the gas has high metallicity. This is especially true at the SDSS spectral resolution, where individual components of Mg II absorption lines usually cannot be resolved. We will later show clear evidence that refutes any indication of a metallicity bias at  $z < 1.65$ .

In this paper, we present a compilation of low-redshift DLAs that is statistically complete for the purpose of determining neutral gas properties at  $z < 1.65$ . We extend the RTN06 UV-DLA sample with three additional Mg II-selected surveys. The first is our HST ACS-HRC-PR200L prism survey for DLAs in the redshift interval  $0.42 < z < 0.70$ , in which we found 35 high-probability DLA systems, of which 26 formally have  $N_{\text{HI}} \geq 2 \times 10^{20}$  atoms  $\text{cm}^{-2}$  (Turnshek et al. 2015). The second is a *GALaxy Evolution Explorer* (GALEX) archival survey in which we found 3 DLAs (this paper). The third is an HST Cycle 19 survey of 16  $z < 0.4$  Mg II systems that were selected from our MMT survey for Mg II systems (Nestor et al. 2006 and this paper), none of which are DLAs. In all, we now have 369 Mg II systems at  $z < 1.65$  for which UV spectra reveal the nature of the corresponding Ly $\alpha$  line; 70 of these are DLAs. Without the possibility of being able to obtain large samples of UV spectra of quasars in the near future, these results will define the state of the field for some time to come.

We describe the three surveys in more detail in §2. The

statistical properties of neutral gas at  $z < 1.65$  as determined from the updated DLA sample are presented in §3. Potential biases are discussed in §4, and we conclude with a summary in §5. Throughout we assume a “737” cosmology with  $H_0 = 70$  km  $\text{s}^{-1}$   $\text{Mpc}^{-1}$ ,  $\Omega_M = 0.3$ , and  $\Omega_\Lambda = 0.7$ .

## 2 THE UV-DLA SURVEYS

In RTN06 we presented results from searches for DLAs in UV spectra of quasars with low-redshift ( $z < 1.65$ ) Mg II systems. This started as a compilation of Mg II systems from various sources that included those from the literature for which *International Ultraviolet Explorer* (IUE) as well as early HST FOS data were available in the archives (Rao et al. 1995). To this dataset we added Mg II-selected DLA survey results from programs in HST Cycle 6 (Rao & Turnshek 2000) and Cycles 9 and 11 (RTN06), as well as additional results that could be culled from the literature using our SDSS Early Data Release quasar Mg II survey (Nestor et al. 2005, henceforth, NTR05). In all, the RTN06 sample included 41 DLAs found among 197 Mg II systems with  $W_0^{\lambda 2796} \geq 0.3$ . All the DLAs in the sample had  $W_0^{\lambda 2796} \geq 0.6$  Å and 50% of systems with Mg II  $W_0^{\lambda 2796}$  and Fe II  $W_0^{\lambda 2600} > 0.5$  Å were DLAs. We note that in the expanded sample presented here, only one of the 70 DLAs has  $W_0^{\lambda 2796} < 0.6$  Å.

With the 41 DLAs in our Mg II-follow-up sample (RTN06), we showed that the incidence of DLAs, i.e.,  $dn/dz$  or the number of DLAs per unit redshift, which is a product of their volume number density and physical cross-section on the sky, showed no evolution for redshifts  $z < 2$ , but evolved significantly in comparison to the high-redshift DLA results available at the time (Prochaska & Herbert-Fort 2004). On the other hand, the cosmological mass density of neutral gas as traced by the DLAs,  $\Omega_{\text{DLA}}$ , remained constant to within the statistical errors for redshifts  $0.5 < z < 5$ . Our sample also had a higher fraction of high-column density DLAs ( $\log N_{\text{HI}} > 21.5$   $\text{cm}^{-2}$ ), which made the low-redshift column density distribution,  $f(N)$ , flatter at higher column densities in comparison to the distributions at high redshift and  $z = 0$  (Zwaan et al. 2005, henceforth, Z05).

Since then, the  $z > 1.65$  regime has benefited tremendously from the explosive increase in the number of quasar spectra available for blind DLA surveys. The N12 statistical sample now includes 3408 DLAs from SDSS DR9. Of course, there is absolutely no hope for a similarly sized sample in the UV in the foreseeable future. Nevertheless, we can make progress by using the metal-line proxies for DLAs that we have developed. With over 40,000 Mg II systems now identified in SDSS spectra (Quider et al. 2011; Zhu & Menard 2013; Seyffert et al. 2013; Sardane et al. 2017, in prep.), the statistics of Mg II systems are known to high statistical accuracy, with uncertainties most certainly dominated by systematics. As described in RTN06, if the fraction of DLAs in a well-defined Mg II sample is known, then the Mg II statistics can be used to determine the incidence of DLAs. Therefore, the UV surveys that we have carried out in the past (RTN06) and those that we describe below were carefully designed to select Mg II systems that have a high probability of being DLAs. Apart from enabling the statistical properties of DLAs to be determined, these also provide a valuable

resource for follow-up studies of individual neutral gas reservoirs at low redshift. This includes their metallicities, dust contents, molecular fractions, star formation, kinematics, associated galaxies, and clustering as a function of redshift.

## 2.1 The HST ACS Prism Survey

The details of the survey and measurements of absorption lines are presented in Turnshek et al. (2015). Here we briefly describe the survey and its results. When STIS on HST failed in 2004 and COS had yet to be installed, we had the opportunity to make use of the low-resolution ACS-HRC-PR200L prism to perform a survey for DLAs in Mg II systems between redshifts  $0.42 < z < 0.70$ . This redshift interval was chosen because it was well-matched to the sensitivity of the PR200L. Despite the low resolution,  $\sim 200$  at  $1730 \text{ \AA}$  and  $\sim 100$  at  $2070 \text{ \AA}$ , it was still possible to detect and measure Ly $\alpha$  lines with DLA column densities ( $N_{\text{HI}} \geq 2 \times 10^{20}$  atoms  $\text{cm}^{-2}$ ). Equally importantly, it was possible to determine which systems were not DLAs. We found 35 high probability DLAs, which were defined as those absorption lines with measured column densities within  $1\sigma$  of  $1 \times 10^{20}$  atoms  $\text{cm}^{-2}$ . Formally, the sample included 26 DLAs with  $N_{\text{HI}} \geq 2 \times 10^{20}$  atoms  $\text{cm}^{-2}$ . For the 61 Mg II systems with  $W_0^{12796} \geq 0.3 \text{ \AA}$ , the spectrum was of high enough signal-to-noise ratio to definitively conclude that there was no DLA line present at the Mg II redshift. For twelve others, the spectra could not be used to determine the nature of the Ly $\alpha$  line. Among these twelve, we include a Mg II system which could have a very large HI column density,  $N_{\text{HI}} > 2 \times 10^{22}$  atoms  $\text{cm}^{-2}$ ; we don't include this in our sample since its column density cannot be definitively determined from the prism data. Details of this sample are given in tables 1 and 2 from Turnshek et al. (2015).

All the Mg II systems selected for this study had  $W_0^{12796} \geq 1 \text{ \AA}$ . They were selected from an early version of the Pittsburgh SDSS Quasar Mg II Absorption-line Survey Catalog (Quider et al. 2011). A few sightlines had additional Mg II systems with  $0.3 \text{ \AA} < W_0^{12796} < 1 \text{ \AA}$ , and one system had  $W_0^{12796} < 0.3 \text{ \AA}$ . As we explain in §3, this distinction becomes important when assigning a selection criterion to a Mg II system in the calculation of the DLA incidence (see also RTN06).

## 2.2 The GALEX Archival Survey

The GALEX archive of quasar grism spectra is an additional resource that can be used to search for strong absorption features in the UV. Strong Ly $\alpha$  lines can easily be detected in the low-resolution grism data, which have  $\lambda/\Delta\lambda \sim 200$  in the  $1344 - 1786 \text{ \AA}$  FUV band and  $\sim 120$  in the  $1771 - 2831 \text{ \AA}$  NUV band (Morrissey et al. 2007). We cross-matched our DR4, DR7, and DR9 SDSS Mg II catalogs (Quider et al. 2011; Sardane et al. 2017 in prep.), with the GALEX GR6 quasar spectroscopic catalog and found 122 matches of which 60 Mg II systems with  $W_0^{12796} \geq 0.3 \text{ \AA}$  had useful spectra with signal-to-noise ratios greater than  $\sim 3$  near the expected position of the Ly $\alpha$  line. We excluded GO programs in the GALEX archive which specifically targeted high-probability DLAs (e.g., Monier et al. 2009). Of the 60 Mg II systems, 3 are DLAs. Two others were measured to be subDLAs. In

the remaining spectra, it was only possible to definitively conclude that no strong absorption line was present at the expected position of Ly $\alpha$ . These were not DLAs, but the possibility that they could be lower column density subDLAs could not be excluded. Table 1 gives details of the Mg II systems with UV spectra in the GALEX archive.

## 2.3 The MMT-HST COS Survey

Nestor et al. (2006) presented a low-redshift Mg II catalog that was obtained using the MMT blue spectrograph with the aim of extending the Mg II distribution to lower redshifts than accessible with the SDSS. They detected 140 Mg II systems with  $W_0^{12796} \geq 0.1 \text{ \AA}$  at  $z \geq 0.15$ . A sample of  $z_{\text{abs}} \leq 0.4$  systems in UV-bright quasars was then selected for follow up with HST-COS in Cycle 19 (GO 12593, Nestor PI), and one of the aims of CoIs Rao and Turnshek was to characterize the neutral gas properties of the absorbers. Quasars with the possibility of Lyman limits in their spectra due to higher redshift absorption systems were eliminated, as were those with faint (FUV  $> 21.5$ ) or unmeasured GALEX FUV fluxes. Three additional quasar spectra were available in the HST archives for use in the program. Measurements of the Mg II absorbers that can be included in our statistical sample are given in Table 2.

We note that four additional Mg II absorbers that did not satisfy our selection criteria for finding Mg II-selected DLAs in a statistically unbiased way were also observed in GO 12593. One of them has  $W_0^{12796} < 0.3 \text{ \AA}$  and is not a DLA. The other three were not from the MMT survey, but are very strong Mg II absorbers from our SDSS Mg II catalog with  $W_0^{12796} \geq 2 \text{ \AA}$ ; none of these three are part of our unbiased final sample since we never established a  $W_0^{12796} \geq 2 \text{ \AA}$  cut in our DLA surveys. Two of the three were found to be DLAs. The  $z_{\text{abs}} = 0.3955$ ,  $W_0^{12796} = 2.32 \pm 0.04 \text{ \AA}$ , system towards the quasar J123200.02-022404.7 (also known as PKS 1229-02) is a known 21 cm absorber, for which we measure  $N_{\text{HI}} = (5.0 \pm 0.3) \times 10^{20}$  atoms  $\text{cm}^{-2}$ . The other DLA is the  $z_{\text{abs}} = 0.3969$ ,  $W_0^{12796} = 2.23 \pm 0.08 \text{ \AA}$ , system towards the quasar J125142.99+463734.7 with  $N_{\text{HI}} = (3.0 \pm 0.2) \times 10^{20}$  atoms  $\text{cm}^{-2}$ .

## 3 STATISTICAL RESULTS

### 3.1 Defining the MgII-DLA sample

As noted in RTN06, the Mg II systems selected for follow-up observations in the UV were chosen in a variety of ways that evolved over a number of years. Each selection method was unbiased, in that it conformed to specific but well understood criteria based on prior results. Our goal was to thoroughly quantify the probability of finding a DLA as a function of  $W_0^{12796}$  while also finding sufficient numbers of them to determine their statistics and make follow-up observations. The UV surveys that we have undertaken since then were described in §2. Our sample of Mg II systems, which have been followed up in the UV for the purpose of determining whether the system is a DLA, now includes 369 systems with  $W_0^{12796} \geq 0.3 \text{ \AA}$ : 197 systems in the RTN06 sample, 96 systems in the ACS-Prism sample (Turnshek et al. 2015), 60 systems in the GALEX Archival sample (Table 1), and

**Table 1.** The GALEX Archival Sample<sup>a</sup>

Quasar	$z_{em}$	$z_{abs}$	Mg II $W_0^{12796}$ (Å)	Mg II $W_0^{12803}$ (Å)	Mg I $W_0^{12852}$ (Å)	Fe II $W_0^{12600}$ (Å)	$\log N_{\text{H}}^b$ atoms cm <sup>-2</sup>
J020114.3-090958	2.011	1.0023	1.504 ± 0.071	1.366 ± 0.074	0.218 ± 0.067	0.772 ± 0.073	...
J020329.8-091020	1.579	1.2166	0.435 ± 0.041	0.361 ± 0.045	≤ 0.1	0.261 ± 0.049	...
J020502.9-081020	1.293	0.9438	1.165 ± 0.055	0.771 ± 0.050	≤ 0.2	0.365 ± 0.049	...
J020502.9-081020	1.293	0.9612	0.429 ± 0.050	0.201 ± 0.051	≤ 0.2	≤ 0.2	...
J032605.6-064915	1.878	0.8842	0.421 ± 0.074	0.515 ± 0.068	0.027 ± 0.062	≤ 0.2	...
J074358.2+323512	0.906	0.7185	1.750 ± 0.020	1.604 ± 0.021	0.357 ± 0.032	1.267 ± 0.022	...
J074451.3+292005	1.183	1.0628	1.182 ± 0.023	1.111 ± 0.024	0.480 ± 0.026	0.770 ± 0.024	...
J083136.9+035414	1.136	0.824	0.777 ± 0.109	0.741 ± 0.099	≤ 0.3	0.150 ± 0.101	...
J083136.9+035414	1.136	1.0871	0.771 ± 0.118	0.525 ± 0.117	0.058 ± 0.081	0.312 ± 0.097	...
J084539.2+172311	1.295	0.9077	0.571 ± 0.107	0.539 ± 0.076	0.127 ± 0.081	0.110 ± 0.097	...
J100024.6+023149	1.311	0.7314	0.547 ± 0.066	0.436 ± 0.078	0.112 ± 0.075	0.241 ± 0.064	...
J100024.6+023149	1.311	0.9009	1.246 ± 0.071	1.097 ± 0.071	0.451 ± 0.096	0.714 ± 0.071	20.08±0.08
J104245.0+114638	1.080	1.0334	1.252 ± 0.070	1.188 ± 0.061	0.219 ± 0.070	0.831 ± 0.053	...
J104513.8-010246	0.971	0.6212	0.361 ± 0.045	0.221 ± 0.043	0.108 ± 0.038	0.080 ± 0.043	...
J104656.7+054150	1.234	0.7127	1.177 ± 0.058	0.795 ± 0.058	0.246 ± 0.061	0.707 ± 0.055	...
J104840.1+053551	1.973	0.9881	1.189 ± 0.130	0.783 ± 0.129	≤ 0.8	1.039 ± 0.15	...
J104932.2+050532	1.115	0.6626	1.143 ± 0.148	0.919 ± 0.205	0.210 ± 0.153	0.599 ± 0.246	...
J105158.5+590652	1.822	0.8174	1.614 ± 0.091	1.177 ± 0.088	0.260 ± 0.080	0.822 ± 0.094	...
J110211.8+284041	1.747	1.1516	0.847 ± 0.104	0.698 ± 0.116	≤ 0.3	0.574 ± 0.125	20.52±0.08
J113221.9+651813	1.130	0.8333	0.521 ± 0.065	0.633 ± 0.076	0.249 ± 0.060	0.277 ± 0.070	...
J113221.9+651813	1.130	1.0092	1.078 ± 0.076	0.965 ± 0.076	...	0.025 ± 0.057	...
J121054.6+202202	0.979	0.9331	0.403 ± 0.049	0.325 ± 0.056	0.097 ± 0.049	≤ 0.5	...
J121404.1+330945	1.598	0.7546	0.400 ± 0.052	0.185 ± 0.048	0.145 ± 0.112	≤ 0.2	...
J122028.0+092826	1.082	0.8863	0.601 ± 0.070	0.405 ± 0.077	≤ 0.3	0.166 ± 0.071	...
J122031.7+094853	0.991	0.7683	0.543 ± 0.087	0.296 ± 0.072	≤ 0.2	≤ 0.2	...
J122424.4+300125	1.192	0.8246	1.101 ± 0.142	0.753 ± 0.150	0.313 ± 0.149	0.184 ± 0.159	...
J123116.4+120023	1.413	1.0960	0.401 ± 0.040	0.305 ± 0.041	0.049 ± 0.037	0.260 ± 0.037	...
J123508.6+254453	1.019	0.9668	0.381 ± 0.065	0.438 ± 0.065	≤ 0.3	≤ 0.3	...
J123934.1+623320	1.659	0.8832	1.704 ± 0.144	1.240 ± 0.117	≤ 0.45	0.908 ± 0.147	...
J124039.3+084251	1.098	1.0127	1.070 ± 0.073	0.740 ± 0.069	0.235 ± 0.081	0.319 ± 0.072	...
J124025.1+085818	1.269	0.8852	1.713 ± 0.083	1.299 ± 0.100	0.340 ± 0.095	0.887 ± 0.107	...
J124044.6+330348	0.812	0.6119	0.685 ± 0.044	0.693 ± 0.047	0.170 ± 0.053	0.522 ± 0.075	...
J124126.1+615804	1.162	1.1289	3.476 ± 0.092	2.921 ± 0.077	0.386 ± 0.078	2.267 ± 0.073	...
J131218.2+493316	1.620	0.8834	1.124 ± 0.066	0.653 ± 0.067	≤ 0.23	0.212 ± 0.061	...
J132330.5+293320	1.098	1.0449	2.758 ± 0.129	2.560 ± 0.122	0.661 ± 0.160	2.075 ± 0.100	20.54±0.20
J132613.7+285144	1.299	0.9423	0.419 ± 0.053	0.295 ± 0.053	0.171 ± 0.060	0.261 ± 0.049	...
J134917.4+460311	1.704	1.0957	2.115 ± 0.167	2.177 ± 0.161	0.756 ± 0.116	1.451 ± 0.086	...
J140023.1+433852	1.127	0.7220	0.786 ± 0.056	0.506 ± 0.051	0.177 ± 0.053	0.237 ± 0.055	...
J140023.1+433852	1.127	0.9464	0.429 ± 0.054	0.429 ± 0.047	≤ 0.16	0.189 ± 0.047	...
J141549.7+005357	1.042	0.8676	0.373 ± 0.033	0.280 ± 0.033	≤ 0.1	≤ 0.1	...
J141551.1+012242	1.239	0.9612	0.556 ± 0.056	0.351 ± 0.050	0.042 ± 0.048	0.131 ± 0.044	...
J141838.4+522359	1.121	1.0232	1.483 ± 0.121	0.844 ± 0.113	0.138 ± 0.137	0.451 ± 0.088	...
J142315.3+375219	1.823	0.8353	1.922 ± 0.062	1.686 ± 0.068	0.653 ± 0.072	1.400 ± 0.068	...
J142501.4+382101	1.145	0.8212	0.488 ± 0.029	0.413 ± 0.031	≤ 0.1	0.131 ± 0.029	...
J143624.3+353709	0.768	0.3922	1.050 ± 0.164	0.782 ± 0.162	≤ 0.4	...	...
J143617.8+353726	1.448	0.8185	0.910 ± 0.148	0.676 ± 0.119	≤ 0.4	≤ 0.3	...
J144313.3+094910	1.192	0.9260	0.934 ± 0.035	0.594 ± 0.034	0.142 ± 0.038	0.316 ± 0.035	19.90±0.11
J153658.3+343149	0.890	0.8080	1.435 ± 0.115	0.801 ± 0.127	0.562 ± 0.117	0.698 ± 0.110	20.48±0.15
J155251.3+314944	1.036	1.0023	1.513 ± 0.027	1.256 ± 0.029	0.202 ± 0.044	0.745 ± 0.032	...
J155454.8+110943	2.327	0.8402	0.652 ± 0.064	0.430 ± 0.054	0.126 ± 0.106	0.310 ± 0.090	...
J160714.1+492331	0.887	0.8410	0.373 ± 0.037	0.288 ± 0.038	...	0.086 ± 0.039	...
J160839.1+354226	1.042	0.7851	1.029 ± 0.044	0.748 ± 0.049	0.267 ± 0.075	0.411 ± 0.058	...
J160855.4+435259	0.933	0.7195	0.608 ± 0.044	0.456 ± 0.040	0.091 ± 0.046	0.266 ± 0.042	...
J160919.0+434727	1.211	1.1362	0.934 ± 0.112	0.530 ± 0.102	0.125 ± 0.082	0.183 ± 0.084	...
J161817.7+330900	1.147	0.8883	0.417 ± 0.032	0.267 ± 0.035	0.048 ± 0.036	0.112 ± 0.032	...
J161902.5+303051	1.288	1.0635	0.801 ± 0.026	0.684 ± 0.026	0.136 ± 0.030	0.302 ± 0.028	...
J171748.4+594820	0.763	0.3745	0.657 ± 0.137	0.677 ± 0.118	0.089 ± 0.081	...	...
J171748.4+594820	0.763	0.6078	0.332 ± 0.067	0.209 ± 0.054	≤ 0.2	≤ 0.2	...
J213042.3+003632	1.263	0.7771	1.569 ± 0.105	1.192 ± 0.130	0.135 ± 0.111	0.537 ± 0.097	...
J235731.7-101507	1.290	0.8809	1.542 ± 0.055	1.556 ± 0.055	0.288 ± 0.067	1.083 ± 0.062	...

<sup>a</sup>Where indicated, upper limits are given at the 3 $\sigma$  level.<sup>b</sup>Blank entries indicate that the Ly $\alpha$  line could not be measured, but is certainly not strong enough to be a DLA.

**Table 2.** The  $z_{abs} \leq 0.4$  MMT-HST COS Sample

Quasar	$z_{em}$	$z_{abs}$	Mg II $W_0^{\lambda 2796}$ (Å)	Mg II $W_0^{\lambda 2803}$ (Å)	Mg I $W_0^{\lambda 2852}$ (Å)	$\log N_{\text{HI}}$ atoms $\text{cm}^{-2}$
J092554.70+400414.1	0.471	0.2471	0.966±0.044	0.850±0.043	0.289±0.051	19.55±0.15 <sup>a</sup>
J094907.16+544510.5	1.369	0.3146	0.813±0.081	0.626±0.087	0.222±0.117	19.08±0.09
J094930.30−051454.0	1.098	0.1973	1.226±0.108	1.015±0.108	0.143±0.093	19.36±0.09
J095000.73+483129.3	0.589	0.2117	0.578±0.063	0.398±0.063	0.096±0.057	16.18±0.06 <sup>b</sup>
J095837.58+555053.1	1.021	0.2511	0.696±0.099	0.313±0.102	0.228±0.097	18.93±0.03
J100102.55+594414.3	0.752	0.3033	1.687±0.020	1.430±0.022	0.261±0.027	19.32±0.10 <sup>a</sup>
J100736.06+363859.6	1.034	0.2106	0.473±0.056	0.307±0.057	0.096±0.065	18.85±0.06
J101703.49+592428.7	0.851	0.4039	0.675±0.052	0.554±0.041	0.083±0.039	18.90±0.08
J102117.47+343721.7	1.404	0.2611	2.158±0.045	1.786±0.049	0.312±0.059	19.30±0.10
J102237.42+393150.5	0.605	0.2520	0.995±0.060	0.689±0.064	0.123±0.068	18.95±0.10
J132325.25+343059.3	0.444	0.3529	0.889±0.048	0.666±0.038	0.279±0.040	19.23±0.08
J132815.61+524403.8	1.341	0.2683	0.300±0.046	0.193±0.044	$\leq 0.15^c$	18.40±0.20
J140035.92+553534.4	0.835	0.3648	3.184±0.029	3.073±0.029	0.425±0.043	20.00±0.11
J141036.81+295550.9	0.570	0.3570	0.633±0.067	0.351±0.053	0.108±0.058	18.70±0.15
J165931.93+373529.0	0.775	0.1994	0.842±0.066	0.795±0.078	0.276±0.069	19.30±0.15
J215647.46+224249.9	1.290	0.3648	0.912±0.012	0.740±0.013	0.083±0.013	18.70±0.17

<sup>a</sup>From Battisti et al. (2012).<sup>b</sup>From Tumlinson et al. (2013).<sup>c</sup>3 $\sigma$  upper limit

16 systems in the MMT-HST sample (Table 2). This search has yielded 70 DLAs, which is the largest unbiased sample of low-redshift DLAs that has been assembled for cosmological studies, but which still pales in comparison to the statistical sample of 3408 DLAs (out of over 6800 DLAs in total) in the high redshift sample of N12.

We use the same methodology to estimate the statistical properties of DLAs as described in RTN06, which we briefly summarize here. The initial searches for UV DLAs were in strong Mg II systems with  $W_0^{\lambda 2796} \geq 0.3$  Å; this matched the Mg II survey threshold of Steidel & Sargent (1992). We adopted this because, with the statistical incidence of Mg II systems known from the Steidel & Sargent (1992) survey, we could use the fraction of DLAs in a well-defined Mg II sample to bootstrap from the Mg II incidence to obtain the DLA incidence. At the time, it was also known that all high-redshift, optically identified DLAs, had Mg II absorption that met this threshold. Based on the results from our archival survey, our earliest non-archival HST surveys, which involved obtaining new HST observations and described in RTN06, had Mg II thresholds of  $W_0^{\lambda 2796} \geq 0.6$  Å. We also used the strength of Fe II to further define subsamples where the DLA fraction would be high. Refining our sample selection in this manner ensured that we used HST time with the maximum efficiency possible in searching for the rare, low-redshift DLAs. Then, with the HST ACS-Prism survey, we selected systems with  $W_0^{\lambda 2796} \geq 1.0$  Å, but no Fe II selection criterion. Since the number of GALEX spectra available in the archives is small, we did not place further constraints on the Mg II systems in the GALEX sample, but simply searched for DLAs in  $W_0^{\lambda 2796} \geq 0.3$  Å systems. The MMT-HST survey sample also had a  $W_0^{\lambda 2796} \geq 0.3$  Å threshold.

We define these subsamples as follows:

1.  $W_0^{\lambda 2796} \geq 0.3$  Å;
2.  $W_0^{\lambda 2796} \geq 0.6$  Å;
3.  $W_0^{\lambda 2796} \geq 0.6$  Å and  $W_0^{\lambda 2600} \geq 0.5$  Å;

4.  $W_0^{\lambda 2796} \geq 1.0$  Å and  $W_0^{\lambda 2600} \geq 0.5$  Å; and
5.  $W_0^{\lambda 2796} \geq 1.0$  Å

Subsample 1 includes all systems surveyed in our initial archival survey (Rao & Turnshek 2000), the GALEX archival sample, and the MMT-HST COS sample. It also includes any additional systems that happened to fall along quasar sightlines that were targeted due to the presence of another stronger system from subsamples 2, 3, 4, or 5. Subsamples 2 and 3 were mainly targeted for observation in HST-Cycle 9, and subsample 4 includes systems found in SDSS-EDR spectra and observed in HST-Cycle 11. A few systems from the SDSS-EDR sample have strong Mg II and Fe II, but have  $W_0^{\lambda 2796} \lesssim 1.0$  Å; these belong in subsample 3. The ACS-Prism sample belongs in subsample 5. The reader is referred to Turnshek et al. (2015) for the Mg II systems in this sample; we do not reproduce it here. The reason for carefully defining these subsamples is that the calculation of DLA incidence is based on the Mg II incidence, and the incidence of Mg II is rest equivalent width-dependent, which is considered in §3.2.

Figure 1 shows the distribution of Mg II rest equivalent widths in our sample. The DLAs are shaded in blue. We note that the lowest rest equivalent width bin,  $0.3 \text{ Å} \leq W_0^{\lambda 2796} < 0.6 \text{ Å}$ , now has one DLA among 70 Mg II systems, whereas the RTN06 sample had none. The fraction of DLAs as a function of  $W_0^{\lambda 2796}$  increases from 1.4% in the lowest  $W_0^{\lambda 2796}$  bin to 67% in the bin centred at  $W_0^{\lambda 2796} = 3.15$  Å. See Figure 2, where Poisson errors with 68% confidence limits are plotted. The last bin from Figure 1 with  $3.3 \text{ Å} \leq W_0^{\lambda 2796} < 3.6 \text{ Å}$  is not plotted in Figure 2. It includes one Mg II system which is not a DLA.

### 3.2 The cosmic incidence of neutral gas, $n_{\text{DLA}}$

The following is adapted from RTN06. The redshift number density of DLAs,  $n_{\text{DLA}}(z)$ , can be determined using the

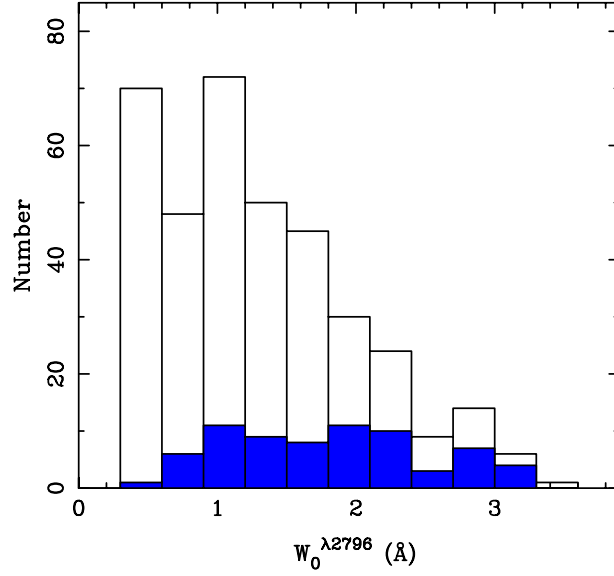


**Figure 1.** Histogram showing the distribution of Mg II rest equivalent widths in our sample. The DLAs are the solid blue histogram.

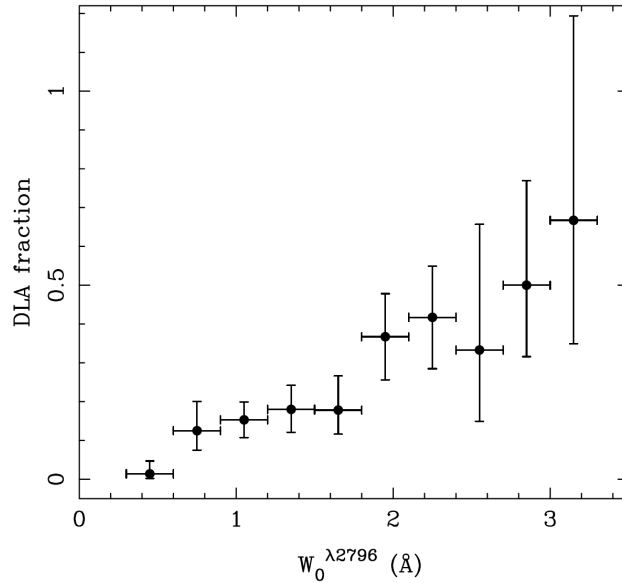


**Figure 2.** The fraction of Mg II systems that are DLAs, which can also be interpreted as the probability of a Mg II system being a DLA, as a function of  $W_0^{\lambda 2796}$ .

equation

$$n_{\text{DLA}}(z) = \eta(z) n_{\text{MgII}}(z), \quad (1)$$

where  $\eta(z)$  is the fraction of DLAs in a Mg II sample as a function of redshift and  $n_{\text{MgII}}(z)$  is the redshift number density of Mg II systems. Since our Mg II sample was assembled under various selection criteria (see §3.1),  $n_{\text{MgII}}(z)$  needs to be evaluated carefully. We can express  $n_{\text{MgII}}(z)$  for our sample as

$$n_{\text{MgII}}(z) = \frac{1}{369} \sum_i w_i n_{\text{MgII}_i}(z), \quad (2)$$

where the sum is over all 369 systems,  $w_i$  is a weighting factor that depends on the  $i^{\text{th}}$  system's selection criterion for

being included in the survey, and  $n_{\text{MgII}_i}(z)$  is the  $i^{\text{th}}$  system's  $dn/dz$  value calculated using the parametrization derived in NTR05 and updated in Sardane et al. (2017, in prep.):

$$dn/dz = N^* (1+z)^\alpha e^{-\frac{W_0}{W^*}(1+z)^{-\beta}}, \quad (3)$$

where  $W_0 \equiv W_0^{\lambda 2796}$  is defined for simplicity and  $N^*$ ,  $W^*$ ,  $\alpha$ , and  $\beta$  are constants. In this expression,  $dn/dz$  is the integrated redshift number density over all  $W_0$  greater than the threshold  $W_0$ . For our calculation, the threshold  $W_0$  is different for each of the five subsamples that comprise our total sample (see §3.1 and RTN06). Thus, for example, a system that belongs to subsample 1 has a threshold of  $W_0 = 0.3 \text{\AA}$  in Equation 3 and a weight of  $w_i = 1$  in Equation 2, while a sys-

tem in subsample 2 has a threshold of  $W_0 = 0.6 \text{ \AA}$  and  $w_i = 1$ , and a system in subsample 5 has a threshold of  $W_0 = 1.0 \text{ \AA}$  and  $w_i = 1$ . This follows since subsamples 1, 2, and 5 are purely Mg II selected without regard to the strength or presence of the Fe II  $\lambda 2600$  line. On the other hand, a system that belongs to subsample 3 has a threshold of  $W_0 = 0.6 \text{ \AA}$  and  $w_i = 0.54$ . This is because a Fe II  $\lambda 2600$  criterion was used to select systems in addition to using a  $W_0$  threshold, and 54% of the 1,130 systems with  $W_0 \geq 0.6 \text{ \AA}$  in the Mg II survey of NTR05 have  $W_0^{\lambda 2600} \geq 0.5 \text{ \AA}$ . Similarly, for systems in subsample 4 we have a threshold of  $W_0 = 1.0 \text{ \AA}$  and  $w_i = 0.72$  because 72% of the 781 systems with  $W_0 \geq 1.0 \text{ \AA}$  in the Mg II survey of NTR05 have  $W_0^{\lambda 2600} \geq 0.5 \text{ \AA}$ . For subsamples 3 and 4 we have assumed that the fraction of Mg II systems that are also strong Fe II systems is independent of redshift.

We have determined the Mg II parametrization for our updated SDSS DR4+DR7 Mg II catalog (Sardane et al. 2017, in prep.), and the values for the constants in Equation 3 are as follows:  $N^* = 1.015 \pm 0.006$ ,  $W^* = 0.442 \pm 0.007$ ,  $\alpha = 0.044 \pm 0.011$ , and  $\beta = 0.618 \pm 0.011$ . These are consistent with the NTR05 values to within the errors. For redshifts  $0.1 < z < 0.36$ , our MMT survey for Mg II systems (Nestor 2004; Nestor et al. 2006) showed that the parametrization of the evolution of  $W_0$  is consistent with that found for the  $z > 0.36$  SDSS Mg II systems with  $W_0 \geq 0.3 \text{ \AA}$  and  $W_0 \geq 0.6 \text{ \AA}$ . We therefore use Equation 3 with the above parameters for the entire redshift range of our sample ( $0.11 < z < 1.65$ ).

Using the formalism described above, we find  $n_{\text{DLA}}(z)$  values as given in Table 3 and plotted as solid black squares in Figures 3 and 4. The redshift intervals were selected to include approximately equal numbers of Mg II systems in each bin. Figure 3 also shows data from the literature as described in the legend. We chose to plot  $n_{\text{DLA}}(z)$  as a function of time to highlight the large cosmic time interval probed by UV DLA surveys. While the general trend of these results indicates a steep decline in the cross-section of DLA absorbers from redshifts 5 to 2, there is less agreement among the various studies at low redshift because of small sample sizes. For example, Meiring et al. (2011) found 3 serendipitous DLAs in the COS-Halos survey (the grey diamond in Figure 3); Neeleman et al. (2016) identified 4 DLAs in a blind survey of 463 quasars in the HST archives (the orange triangle). The blue cross is a 21 cm follow-up study of Mg II systems by Kanekar et al. (2009) in which they found 9 detections of 21 cm absorption among 55 Mg II systems. The red open squares are our previous results which included 41 DLAs in 197 Mg II systems (RTN06). The solid black squares are results from our current sample and include 70 DLAs in 369 Mg II systems. These new data confirm that the decline in DLA absorber cross-section continues to occur between redshifts  $z = 2$  to  $z = 0$ .

In Figure 4 we only plot data with the smallest uncertainties in each redshift regime. At high redshifts these are the SDSS DR9 results from N12, who correct for incompleteness and false identifications in previous studies. The recent results of Sánchez-Ramírez et al. (2016) for redshifts  $1.6 < z < 5$  are consistent with the N12 results, albeit with larger uncertainties. The  $z = 0$  data points are from Z05, who used *Westerbork Synthesis Radio Telescope* H I maps of a large sample of nearby galaxies to estimate  $n_{\text{DLA}}(z)$ , and Braun (2012, henceforth B12) who used extremely high-

resolution maps of Local Group galaxies and the local galaxy H I mass function to calculate the H I cross section as a function of  $N_{\text{HI}}$  after accounting for 21 cm beam size and opacity effects. The discrepancy between these two local estimates using 21 cm emission is almost a factor of two:  $0.045 \pm 0.006$  versus  $0.026 \pm 0.003$  from Z05 and B12, respectively. With the uncertainties in the  $z > 0$  data having improved considerably, we can now use these data to help inform and possibly constrain the  $z \sim 0$  values of  $n_{\text{DLA}}$ . We show three power-law fits to the data in Figure 4. The red curve is a fit to the eight  $z > 0$  data points and the Z05 data point (dark blue triangle), the green curve is a fit that includes the  $z > 0$  data points and the B12 data point (light blue star), and the black curve is a fit to the  $z > 0$  data points alone. The fits are of the form

$$n_{\text{DLA}}(z) = n_0(1+z)^\gamma, \quad (4)$$

where  $n_0 = 0.035 \pm 0.007$  and  $\gamma = 1.488 \pm 0.151$  for the  $z > 0$  + Z05 data points,  $n_0 = 0.026 \pm 0.004$  and  $\gamma = 1.707 \pm 0.108$  for the  $z > 0$  + B12 data points, and  $n_0 = 0.027 \pm 0.007$  and  $\gamma = 1.682 \pm 0.200$  for the  $z > 0$  data points alone.

Extrapolation of the  $z > 0$  fit down to  $z = 0$  clearly favors the B12 determination of  $n_{\text{DLA}}$ . All three fits are consistent with the  $z > 3.5$  data points shown in Figure 3. The  $z > 0$  power law is what we report for the form of the evolution of the incidence of neutral gas DLAs as a function of redshift for  $0 < z < 5$ , i.e.,

$$n_{\text{DLA}}(z) = (0.027 \pm 0.007)(1+z)^{(1.682 \pm 0.200)}. \quad (5)$$

### 3.3 The cosmic mass density of neutral gas, $\Omega_{\text{DLA}}$

We compute  $\Omega_{\text{DLA}}$  as before (RTN06). DLA column density measurements,  $N_{\text{HI}}$ , and the incidence of DLAs,  $n_{\text{DLA}}(z)$ , can be used to determine  $\Omega_{\text{DLA}}(z)$  via the expression

$$\Omega_{\text{DLA}}(z) = \frac{\mu m_{\text{H}}}{\rho_c} \frac{H_0}{c} n_{\text{DLA}}(z) \langle N_{\text{HI}} \rangle \frac{E(z)}{(1+z)^2}, \quad (6)$$

where

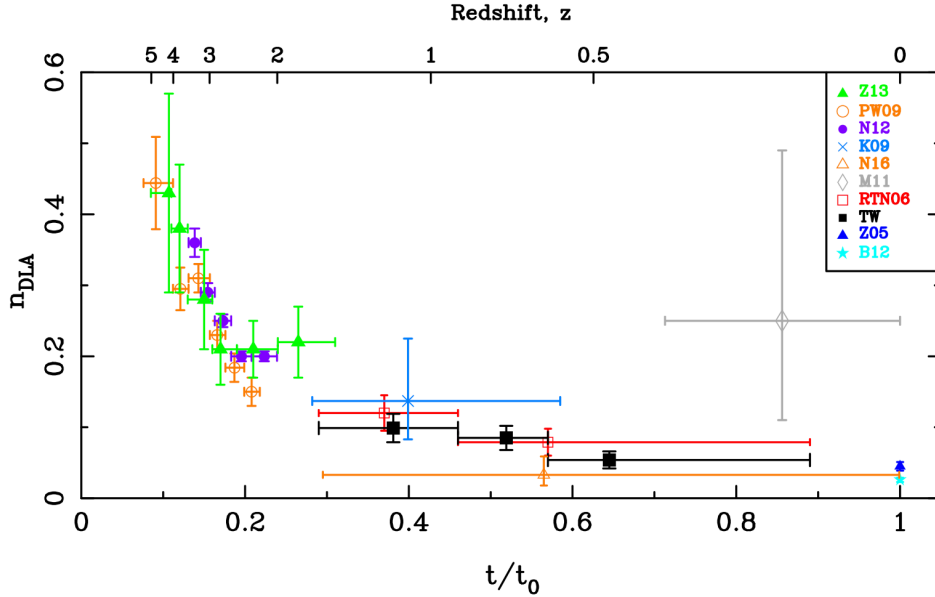
$$E(z) = (\Omega_{\text{M}}(1+z)^3 + (1 - \Omega_{\text{M}} - \Omega_{\Lambda})(1+z)^2 + \Omega_{\Lambda})^{1/2}. \quad (7)$$

Again, the “737” cosmology is used to calculate  $\Omega_{\text{DLA}}$ . Also,  $\mu = 1.3$  corrects for a neutral gas composition of 75% H and 25% He by mass,  $m_{\text{H}}$  is the mass of the hydrogen atom,  $\rho_c$  is the critical mass density of the universe, and  $\langle N_{\text{HI}} \rangle$  is the mean  $N_{\text{HI}}$  of DLAs in each redshift bin. The mean  $N_{\text{HI}}$  and  $\Omega_{\text{DLA}}$  values calculated in the same three redshift bins as  $n_{\text{DLA}}(z)$  are given in Table 3. Figure 5 is a plot of our current results, shown as solid black squares, as well as various results from the literature. The references are given in the captions to Figures 3 and 5. The large scatter in the various determinations of  $\Omega_{\text{DLA}}$  is remarkable and highlights the inherent difficulty in estimating  $\Omega_{\text{DLA}}$ , which is primarily due to small sample sizes and the fact that the mean H I column density of a sample is dominated by the highest (and rarest) column density systems.

A comparison of our previous results on  $\Omega_{\text{DLA}}$  (RTN06), shown as open red squares in Figure 5, with our current results shows that  $\Omega_{\text{DLA}}$  in the UV regime is now somewhat smaller, although the two determinations are consistent within the errors. As we show in §3.4, this is due to the fact that our previous sample had a higher fraction of high

**Table 3.** UV-DLA statistics:  $n_{\text{DLA}}(z)$  and  $\Omega_{\text{DLA}}(z)$ 

Redshift Interval	Mean $z$	$n_{\text{DLA}}(z)$	$\langle N_{\text{HI}} \rangle^a$ ( $\text{cm}^{-2}$ )	$\Omega_{\text{DLA}}(z)$
0.11 - 0.61	0.464	$0.054 \pm 0.012$	$(1.32 \pm 0.34) \times 10^{21}$	$(7.7 \pm 2.6) \times 10^{-4}$
0.61 - 0.89	0.731	$0.085 \pm 0.017$	$(8.75 \pm 1.34) \times 10^{20}$	$(6.7 \pm 1.6) \times 10^{-4}$
0.89 - 1.65	1.172	$0.099 \pm 0.020$	$(1.02 \pm 0.22) \times 10^{21}$	$(7.5 \pm 2.9) \times 10^{-4}$

<sup>a</sup>Bootstrap errors are reported.**Figure 3.** Redshift number density of DLAs,  $n_{\text{DLA}}(z)$  plotted as a function of cosmic time with  $t = t_0$  being the present epoch. Redshifts are noted along the top axis. A few key results from the literature are also plotted. References in the legend are as follows: Z13: Zafar et al. (2013); PW09: Prochaska & Wolfe (2009); N12: Noterdaeme et al. (2012); K09: Kanekar et al. (2009); N16: Neeleman et al. (2016); M11: Meiring et al. (2011); RTN06: Rao, Turnshek, & Nestor (2006); TW: this work; Z05: Zwaan et al. (2005); B12: Braun (2012).

column density systems, which skewed the column density distribution function higher for  $\log N_{\text{HI}} > 21.5$ , but leaving it within  $2\sigma$  of the high-redshift data. Now, with a sample that's nearly twice as large, we no longer see evidence of this. This result illustrates the fact that the value of  $\Omega_{\text{DLA}}$  is dominated by the highest column densities in the sample, and minor changes in the column density distribution at the high  $N_{\text{HI}}$  end can affect  $\Omega_{\text{DLA}}$ . Thus, it is probably worth noting that our previous value of  $\Omega_{\text{DLA}}$  (RTN06) was never “biased high” by our Mg II-selection methods. Instead it should be recognized that small number statistics at the high  $N_{\text{HI}}$  end lead to significant uncertainties; these uncertainties at low redshift can be reduced by measuring larger samples of Mg II-selected DLAs.

In Figure 6 we plot only one set of results for each redshift range: Crighton et al. (2015) for  $z \geq 4$ , N12 for  $2 < z < 3.5$ , our current results for  $0.11 < z < 1.65$ , the Hoppmann et al. (2015) data point that is a combined estimate for all 21 cm emission results for  $0 < z < 0.2$  but which does not include the Braun (2012) result, and the Braun (2012) data point.

As we did for  $n_{\text{DLA}}(z)$ , we fit a power law to only the N12 data points and our current results. We derive

$$\Omega_{\text{DLA}}(z) = (4.77 \pm 1.60) \times 10^{-4} (1+z)^{(0.64 \pm 0.27)}, \quad (8)$$

which is shown as the solid curve in Figure 6. We extrapolate this curve to  $z = 0$ , but it is clear that the uncertainties in the low-redshift data points are such that no conclusion should be drawn as to how the  $z > 0$  DLA results may inform or constrain the 21 cm emission results at  $z = 0$ , unlike extrapolation of the  $n_{\text{DLA}}(z)$  fit to  $z = 0$  (Figure 4.)

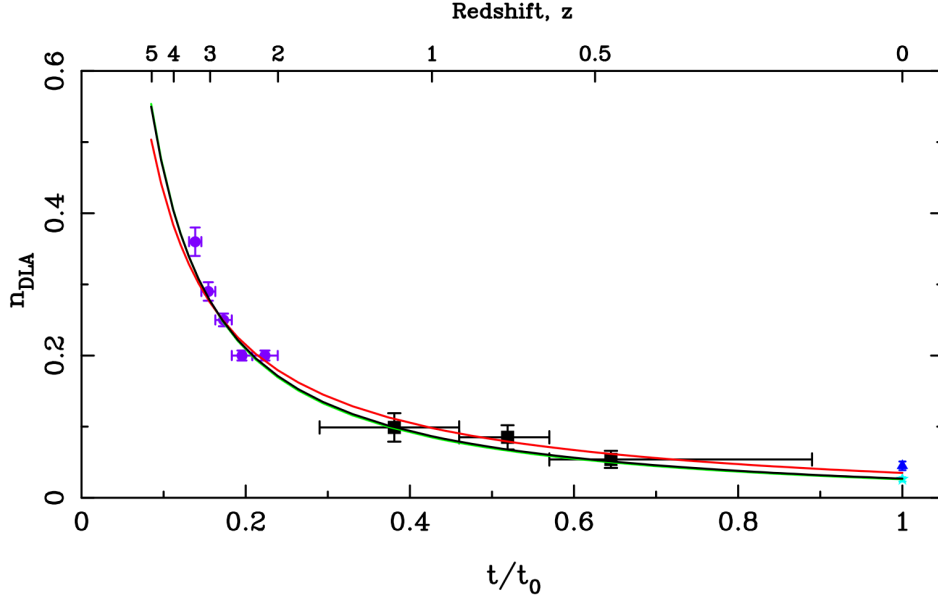
### 3.4 The DLA column density distribution, $f(N)$

Figure 7 is a plot of the column density distribution of DLAs. The black solid squares were calculated using the expression

$$f(N, z) = n_{\text{DLA}}(z) \frac{E(z)}{(1+z)^2} \frac{y(N, z)}{\Delta N}, \quad (9)$$

where  $y(N, z)$  is the fraction of DLAs with column densities between  $N$  and  $N + \Delta N$  at redshift  $z$ , and  $E(z)$  is given by Equation 7, as was the case in RTN06. The  $f(N)$  values, listed in Table 4, were calculated at the mean redshift of our total sample,  $\langle z \rangle = 0.789$ , and using the redshift number density of DLAs for all systems in the redshift interval  $0.11 < z < 1.65$ ,  $n_{\text{DLA}}(z) = 0.078 \pm 0.009$ . The black solid line in Figure 7 is a fit to the data points and has a slope of  $-1.46 \pm 0.20$ . A comparison with our previous results from RTN06 shows only minor differences, with the largest devi-





**Figure 4.** Same as Figure 3, but only the lowest uncertainty studies in the high- and low-redshift regimes are retained. The  $z > 2$  data are from Noterdaeme et al. (2012) and the black squares are this work. The  $z = 0$  data points are from Z05 (dark blue triangle) and B12 (light blue star). The three curves are power law fits to the data of the form described in the text. The red curve includes the  $z > 0$  data points and the Z05 data point, the green curve includes the  $z > 0$  data points and the B12 data point, and the black curve includes only the  $z > 0$  data points. Note that the black and green curves very nearly overlap.

**Table 4.**  $f(N)$  at  $\langle z \rangle = 0.8$

$\log N_{\text{HI}}$ range	$\log f(N)$
20.3 – 20.6	$-22.31^{+0.10}_{-0.13}$
20.6 – 20.9	$-22.45^{+0.09}_{-0.11}$
20.9 – 21.2	$-23.09 \pm 0.14$
21.2 – 21.5	$-23.56^{+0.15}_{-0.19}$
21.5 – 21.8	$-23.99 \pm 0.20$

ation being in the last  $\log N_{\text{HI}}$  bin. The higher fraction of high column density systems that we noted in RTN06 has now disappeared. The current  $f(N)$  value in our highest  $N_{\text{HI}}$  bin is consistent with both the high-redshift value of N12 and the  $z = 0$  value of B12. (Other more recent estimates of  $f(N)$  at high redshift are consistent with the N12 results, but have larger error bars due to smaller samples, and we do not plot them here.) We have not detected any systems with  $\log N_{\text{HI}} > 21.8 \text{ cm}^{-2}$ , and therefore cannot comment on the high- $N_{\text{HI}}$  tail of the  $f(N)$  distribution at low redshift beyond this value. Nonetheless, the high  $N_{\text{HI}}$  end of the  $f(N)$  distribution appears not to have evolved with redshift, while the low  $N_{\text{HI}}$  end, on the other hand, is significantly different in all three redshift regimes if the B12 data are used at  $z = 0$ . If the Z05 result is used instead, then the  $f(N)$  distributions diverge at both ends: the low-redshift data points from the other two at low values of  $N_{\text{HI}}$  and the  $z = 0$  curve from the other two at high values of  $N_{\text{HI}}$ . The interpretation of these trends requires better data, or better understanding of the data, surprisingly, at  $z = 0$ . The B12 work highlights the need for caution when interpreting 21 cm maps of galaxies in terms of quasar absorption line information, and this caution applies both at high and low HI column densities. At

the high  $N_{\text{HI}}$  end, since the conversion of 21 cm brightness temperature assumes that the gas is in the optically thin regime, the true value of  $N_{\text{HI}}$  may be higher than estimated from emission maps due to saturation effects. At the low column density end, higher resolution 21 cm maps ( $\sim 100$  pc for the B12 data versus 1.4 kpc for the Z05 data), which better approximate quasar pencil beam surveys, show a decrease in the relative numbers of low- $N_{\text{HI}}$  sightlines. This is likely due to the presence of higher column density gas within larger beams. However, since the B12 results were estimated based on a scaling of the properties of three Local Group galaxies to the HI mass function of the local universe, there may be systematic uncertainties in the overall normalization of the derived cosmological parameters.

#### 4 ON THE Mg II SELECTION METHOD

One often-noted concern about using the Mg II-selection method to conduct a UV survey for DLAs is that it may preferentially select systems with higher metallicities, and that we might be missing lower metallicity DLAs which would show up as systems with  $W_0^{2796} < 0.3 \text{ \AA}$ , or perhaps they might have no detectable Mg II absorption. Another concern

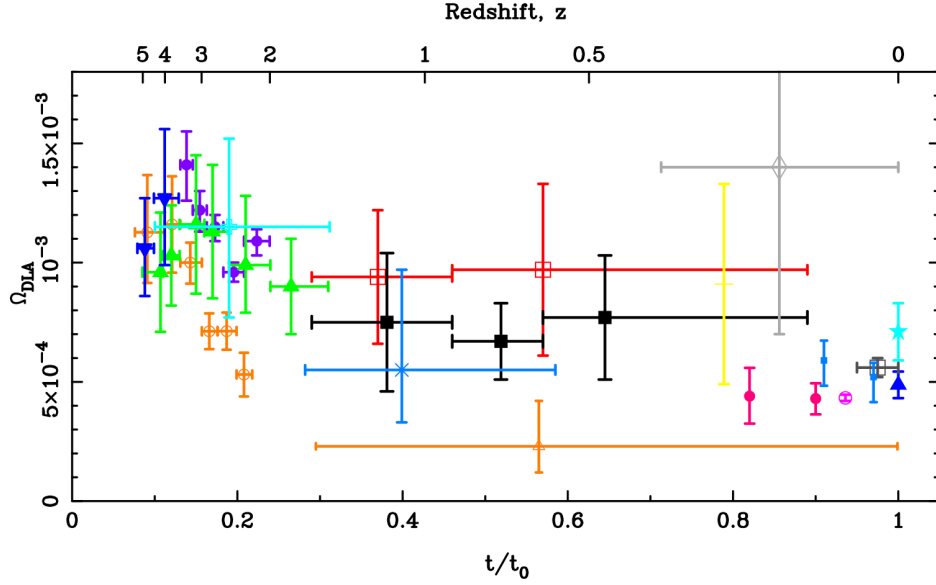


**Figure 5.** The cosmological mass density of neutral gas as measured by DLAs,  $\Omega_{\text{DLA}}$ , plotted as a function of cosmic time with  $t = t_0$  being the present epoch. Redshifts are noted along the top axis. Many notable results from the literature are also plotted. Those in common with Figure 3 are plotted with the same symbols and colors. Our current results are solid black squares. Many references have been added. (These generally do not quote values for  $n_{\text{DLA}}(z)$ .) From high to low redshift, these are Crighton et al. (2015, dark blue inverted triangles), Jorgenson et al. (2006, light blue open plus), Lah et al. (2007, yellow horizontal bar), Rhee et al. (2013, magenta filled circles), Hoppmann et al. (2015, purple open circle), Delhaize et al. (2013, small solid blue squares), and Martin et al. (2010, dark grey open square). The large scatter among these various determinations highlights the difficulty in accurately measuring  $\Omega_{\text{DLA}}$ .

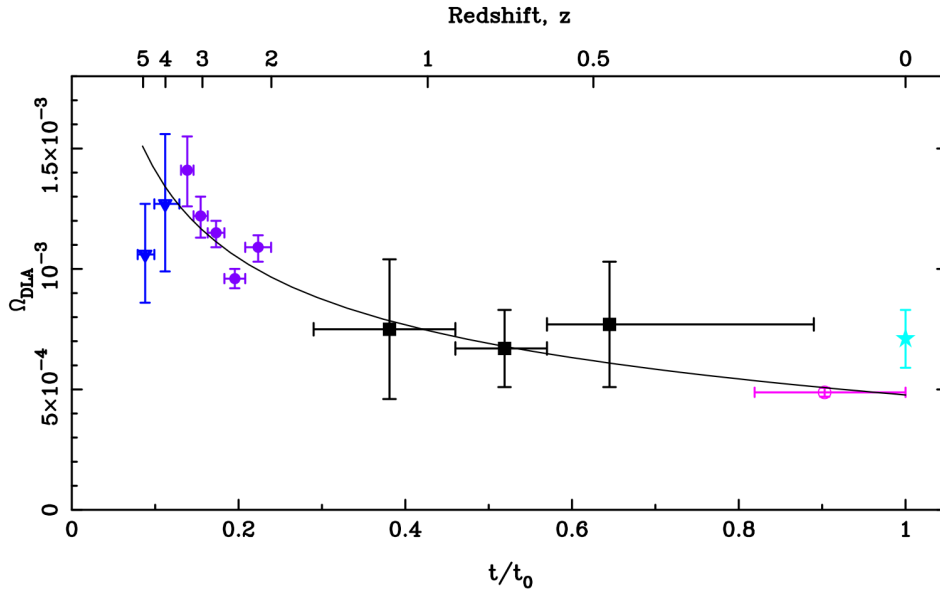


**Figure 6.** Same as Figure 5, but with only the following data plotted: Crighton et al. (2015), N12, this work, Hoppman et al. (2015), and B12. See text. The symbols and colors are the same as in Figure 5. The fit only includes the  $2 < z < 3.5$  data points of N12 and our current results for  $0.11 < z < 1.65$ , and is of the form shown in Equation 8.

has been that by using strong Mg II as a proxy for DLAs, our sample could include a higher fraction of high  $N_{\text{HI}}$  systems, thus causing our derived  $\Omega_{\text{DLA}}$  to be biased high. We address these concerns below in reverse order. In short, there is absolutely no evidence for these effects at  $z < 1.65$ .

#### 4.1 Is $\langle N_{\text{HI}} \rangle$ biased high?

In RTN06 we presented the  $W_0^{2796}$  and  $N_{\text{HI}}$  distributions of our sample of 41 DLAs in 197 Mg II systems, where figures 3 and 4 of RTN06 showed that the fraction of Mg II systems that are DLAs increases with increasing  $W_0^{2796}$ . This result is also true for our current expanded sample (Figure 2). The

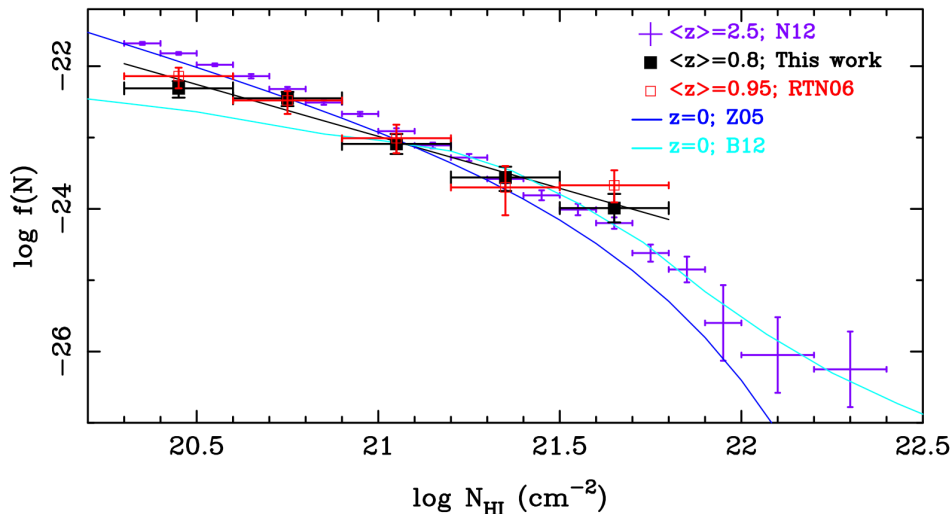


**Figure 7.** The column density distribution of DLAs. Our current results are shown as black squares, with the best-fitting power law shown as the black solid line. The fit has a slope of  $-1.46 \pm 0.20$ . Our earlier RTN06 results are the open red squares; the excess of high  $N_{\text{HI}}$  systems is not seen in the larger updated sample. The low  $N_{\text{HI}}$  tail of the distribution is seen to decrease as one progresses from high redshift (N12), to low redshift (this study), to  $z = 0$  (B12), although to establish this we would need to more clearly understand why the results of Z05 and B12 disagree. At the highest  $N_{\text{HI}}$  values our results are more consistent with both the  $z = 0$  21 cm emission results of B12 as well as the high redshift results of N12.

data points in figure 4 of RTN06 showed that the mean  $N_{\text{HI}}$  value,  $\langle N_{\text{HI}} \rangle$ , for all the Mg II systems (DLAs and non-DLAs) remains constant as a function of  $W_0^{\lambda 2796}$  for  $W_0^{\lambda 2796} \geq 0.6 \text{ \AA}$ . We did not find any DLAs at  $0.3 \text{ \AA} \leq W_0^{\lambda 2796} < 0.6 \text{ \AA}$ <sup>1</sup>. Unfortunately we cannot make a similar plot using *all* of the new Mg II absorbers in our current sample because we do not have measured  $N_{\text{HI}}$  values for most of the new subDLAs. In figure 5 of RTN06 we showed  $\langle N_{\text{HI}} \rangle$  for only DLAs in that sample; it hinted at a *decreasing* trend of  $\langle N_{\text{HI}} \rangle$  with increasing  $W_0^{\lambda 2796}$ , if at all. In fact, the error bars, and the low point in the bin at  $W_0^{\lambda 2796} \sim 1.35 \text{ \AA}$ , showed the mean  $N_{\text{HI}}$  to be consistent with a value of  $\sim 1 \times 10^{21} \text{ cm}^{-2}$  as a function of  $W_0^{\lambda 2796}$ . There was no evidence in the prior data that bins at larger  $W_0^{\lambda 2796}$  had higher  $\langle N_{\text{HI}} \rangle$ . The results did show, of course, a higher probability of larger  $W_0^{\lambda 2796}$  systems hosting a DLA, but the  $\langle N_{\text{HI}} \rangle$  of such DLAs was clearly not higher than the  $\langle N_{\text{HI}} \rangle$  of lower  $W_0^{\lambda 2796}$  DLAs.

The above results remain true for our new, updated sample. Figure 8 shows the plot of  $N_{\text{HI}}$  versus  $W_0^{\lambda 2796}$  for our current sample of 70 DLAs. Once again, there is no evidence for an increasing trend of  $N_{\text{HI}}$  with increasing  $W_0^{\lambda 2796}$ . Also, we now have one system in the updated sample with  $0.3 \text{ \AA} \leq W_0^{\lambda 2796} < 0.6 \text{ \AA}$ , and this system has  $N_{\text{HI}} = (8 \pm 2) \times 10^{20} \text{ cm}^{-2}$ . The red points in Figure 8 are mean values of  $N_{\text{HI}}$  calculated in 10 bins of 7 DLAs each. Bootstrap errors are shown. The solid line is a fit to these data points that has a slope of  $-0.08 \pm 0.05$ , consistent with no correlation between  $\langle N_{\text{HI}} \rangle$  and  $W_0^{\lambda 2796}$ . The grey region represents the 95% confidence band for the fit. We see that the lack of very high  $N_{\text{HI}}$  systems in the top right corner of Figure 8 persists, and is driving

<sup>1</sup> We also reiterate that no DLA has been found with  $W_0^{\lambda 2796} < 0.3 \text{ \AA}$ , and thus, bins with lower values of  $W_0^{\lambda 2796}$  do not contribute to the cosmic neutral-gas density of the universe.

the marginally negative slope, although this is likely to be due to small number statistics.

We should clarify several points. Our latter surveys for DLAs with HST preferentially selected Mg II systems with  $W_0^{\lambda 2796} \geq 0.6 \text{ \AA}$  since results from the initial survey indicated that this would lead to a higher probability of finding a DLA. Then, for example, had there been a positive correlation between  $W_0^{\lambda 2796}$  and  $N_{\text{HI}}$ , this type of selection could have resulted in preferentially finding DLAs with higher values of  $N_{\text{HI}}$ , i.e., when calculating  $\langle N_{\text{HI}} \rangle$  for the entire sample,  $\langle N_{\text{HI}} \rangle$  would have been biased high. Thus, even though  $n_{\text{DLA}}$  would not have been affected (i.e., biased) because it is calculated using the relative incidence of Mg II systems (Equations 2 and 3), the calculation of  $\Omega_{\text{DLA}}$  using Equation 6 would have been biased high had we used a value for  $\langle N_{\text{HI}} \rangle$  that was biased high. To correct for this we would then have needed to calculate  $\Omega_{\text{DLA}}$  in parts as a function of  $W_0^{\lambda 2796}$ . However, as we showed above,  $\langle N_{\text{HI}} \rangle$  is independent of  $W_0^{\lambda 2796}$  for all values of  $W_0^{\lambda 2796}$  where DLAs are detected, and therefore such a “bias” does not exist in our previous sample nor in our new, updated Mg II-selected sample over the redshift interval of  $0.11 < z < 1.65$  (the UV DLA regime). If anything, if the minimal negative correlation shown in Figure 8 is real, it would mean a negative bias at the highest  $W_0^{\lambda 2796}$  values, which would have required a slight (but insignificant) upward correction for  $\Omega_{\text{DLA}}$ .

#### 4.2 Is there a metallicity bias?

Since our selection is based on a ‘metal,’ Mg II, the H I gas that is being traced by Mg II systems is not ‘pristine.’ There must have been an epoch when DLAs were not enriched enough to have Mg II absorption, in which case, our selection method would miss them. There may also be pockets of high-density neutral gas that have very low metallicity at

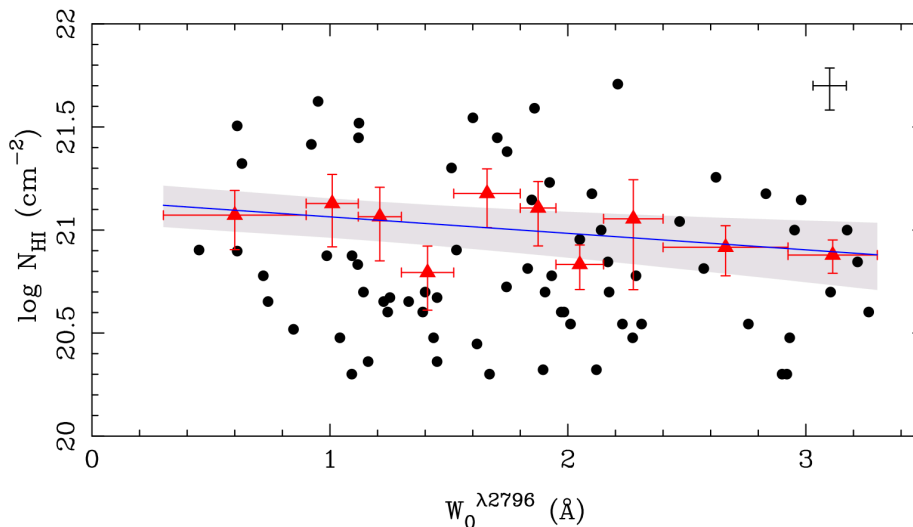


**Figure 8.**  $\log N_{\text{HI}}$  versus  $W_0^{\lambda 2796}$  for the 70 DLAs in our sample. The average error bars of the data points are shown in the top-right corner. Mean H I column densities are shown as red points for 10 bins chosen to have an equal number of DLAs in each bin. Bootstrap errors are shown. The solid line is a fit to these points and has a slope of  $-0.08 \pm 0.05$ . The gray region represents the 95% confidence band for the fit.

redshifts  $z < 1.65$  and which do not have Mg II above the threshold of our survey. These would also be missed. However, there is no evidence for this. All DLAs observed thus far at all redshifts have Mg II or other low ionization absorption (e.g., Turnshek et al. 1989, Lu et al. 1993, Lu & Wolfe 1994, Wolfe et al. 2005). In addition, the high redshift ( $2 < z < 6$ ) Mg II-DLA study of Matejek et al. (2013) has shown that all DLAs in their sample have  $W_0^{\lambda 2796} > 0.4 \text{ \AA}$ . Thus, metal-enrichment existed at the highest redshifts of the DLAs found in their study ( $z \sim 5.3$ ). With its large oscillator strength, the Mg II  $\lambda 2796$  line becomes saturated at relatively low column densities, and thus, its rest equivalent width cannot be used as a measure of metallicity. The DLAs found by Matejek et al. (2013) were measured to have metallicities, e.g.,  $[\text{Si}/\text{H}]$ , with lower limits down to a few thousandths solar, with several lower limits measured at a tenth solar. Thus, there are no known DLAs that are extremely metal poor and that do not show strong Mg II absorption even at the highest redshifts studied thus far. Matejek et al. (2013) also found that the metallicities of these Mg II-DLAs are not different than those of the general population of DLAs at those redshifts, i.e., Mg II selection does not bias the DLA sample towards higher metallicities. They conclude that the observed metallicities are not inconsistent with the hypothesis that the two groups trace the same population of absorbers.

Until recently, almost all of the DLA and sub-DLA metallicity measurements at low redshift were for systems identified in our surveys. These measurements showed that there is a steady increase in the metallicity of the universe from high redshift to the present epoch, and that subDLAs generally have higher metallicities than DLAs (e.g., Kulkarni et al. 2007, 2010, Som et al. 2015, Quiret et al. 2016 and references therein). If there was a metallicity bias in the selection of DLAs and subDLAs at low redshift, then the observed increase in metallicity with time would have to be corrected for this bias. Dessauges-Zavadsky et al. (2009)

speculated that the high metallicities of subDLAs at low redshift were likely due to a bias introduced by our Mg II selection of DLAs and subDLAs. The DLAs in the sample of Nestor et al. (2008) also had higher mean metallicities than non-Mg II selected DLAs by about 0.1 dex. However, the Nestor et al. (2008) sample mainly included systems with  $W_0^{\lambda 2796} > 1 \text{ \AA}$ .

The trend that metallicity increases with  $W_0^{\lambda 2796}$  is well known. Turnshek et al. (2005) used composites of SDSS spectra binned in  $W_0^{\lambda 2796}$  and the mean H I column density for  $W_0^{\lambda 2796} \geq 0.6 \text{ \AA}$  from our HST surveys to show the following: 1) that the mean metallicity of Mg II absorbers increased with increasing  $W_0^{\lambda 2796}$ , 2) that the  $W_0^{\lambda 2796} = 0.6 \text{ \AA}$  systems have a mean metallicity of one-hundredth solar ( $[\text{X}/\text{H}] = -2$ ) and showed little evidence for depletion, and 3) that the amount of depletion increased with increasing  $W_0^{\lambda 2796}$ . Péroux et al. (2003), Ledoux et al. (2006), Meiring et al. (2009), Møller et al. (2013), Som et al. (2015), Quiret et al. (2016), among others, have noted a trend between line widths and metallicity, prompting some to infer a mass-metallicity relation for quasar absorbers similar to what is observed for galaxies. With recent results on Mg II absorbers suggesting that they arise in bipolar outflows (Bouché et al. 2012; Bordoloi et al. 2014), the mass of the host galaxy may not be the only driver of the velocity width - metallicity relation. In any case, whatever the reason for the correlation, it is recognized that the correlation exists. Does this mean that we are missing the lowest metallicity DLAs since our selection has a cut-off at  $W_0^{\lambda 2796} = 0.3 \text{ \AA}$ ?

Since we believe that we have not missed any DLAs through Mg II selection (§4.1), we also have not missed any DLAs with metallicities that are lower than what our current samples measure. One way to investigate whether our Mg II-selected DLAs and subDLAs have higher metallicities, is to compare their metallicities to samples of DLAs that were identified serendipitously. Figure 9 shows metallicity mea-

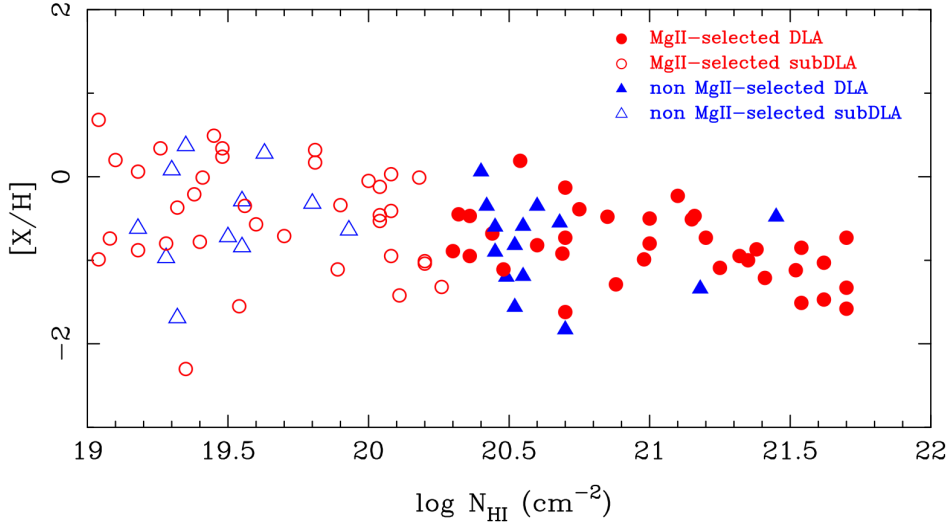


**Figure 9.** Metallicities of DLAs and subDLAs at  $z < 1.65$  versus  $\log N_{\text{HI}}$  column density. Metallicity measurements are from a variety of literature sources. The majority are from Quiret et al. (2016) and references therein. Solid and open red circles are Mg II-selected DLAs and subDLAs, respectively. These include systems from our sample as well as from R. Becker’s Mg II-selected HST DLA survey (GO 9051; Rao et al. 2005; Lacy et al. 2003; Meiring et al. 2006) and a 21 cm-DLA survey of Mg II systems from Ellison et al. (2012). Blue solid and open triangles are non-Mg II-selected DLAs and subDLAs.

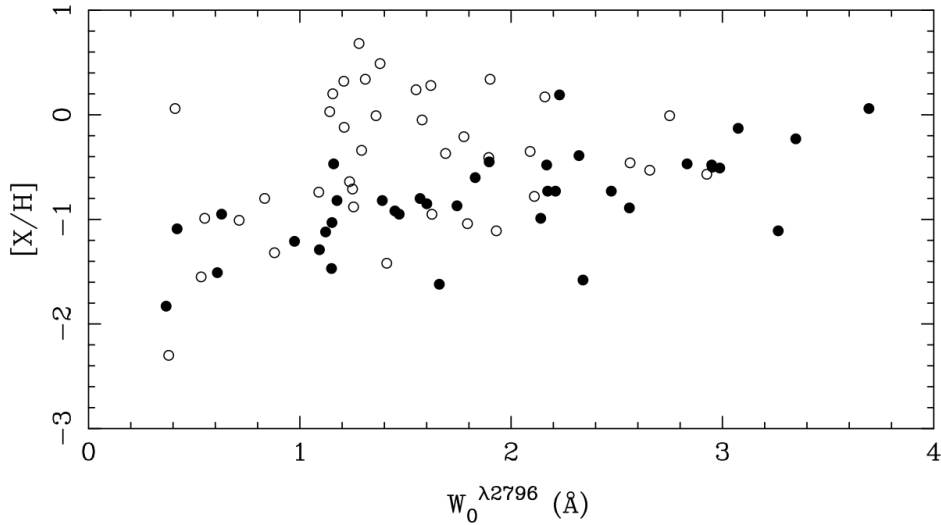


**Figure 10.** Metallicities of DLAs (solid circles) and subDLAs (open circles) at  $z < 1.65$  versus  $W_0^{\lambda 2796}$  rest equivalent width. The well-known increase in metallicity with  $W_0^{\lambda 2796}$  is evident in this sample, with the DLAs showing a tighter correlation. All known DLAs have  $W_0^{\lambda 2796} \geq 0.3 \text{ \AA}$ , and all  $z < 1.65$  DLAs have metallicities  $[X/H] > -2$ . Extrapolation of the DLA metallicity- $W_0^{\lambda 2796}$  correlation to  $W_0^{\lambda 2796} = 0.3 \text{ \AA}$  is consistent with the existence of a floor in DLA  $W_0^{\lambda 2796}$  and  $[X/H]$  values.

measurements of DLAs and subDLAs in Mg II-selected systems and non-Mg II-selected systems at  $z < 1.65$ , i.e., in UV-detected systems. There is now a statistically significant number of non-Mg II-selected DLAs at  $z < 1.65$  for which metallicity measurements exist in the literature to be able to perform this comparison in a meaningful way. The well-known increase in metallicity with decreasing  $N_{\text{HI}}$  is observed in this sample as well. However, there is no evidence that the Mg II-selected DLAs have higher metallicities than the non-Mg II-selected ones. A Kolmogorov-Smirnov (KS) test performed on the two samples gives a  $p$ -value of 0.934, indi-

cating that the two samples are drawn from the same parent population at a high level of confidence.

In Figure 10, we plot the metallicities of DLAs and subDLAs at  $z < 1.65$  as a function of  $W_0^{\lambda 2796}$ . Both Mg II-selected as well as non-Mg II-selected systems are included. (There are a few serendipitously discovered DLAs with measurements of  $W_0^{\lambda 2796}$ .) The trend of increasing metallicity with  $W_0^{\lambda 2796}$  is clear, particularly for the DLAs. There are two points to note from this plot. First, since we have shown that there are no DLAs with  $W_0^{\lambda 2796} < 0.3 \text{ \AA}$ , the trend of metallicity with  $W_0^{\lambda 2796}$  implies that there must be a floor

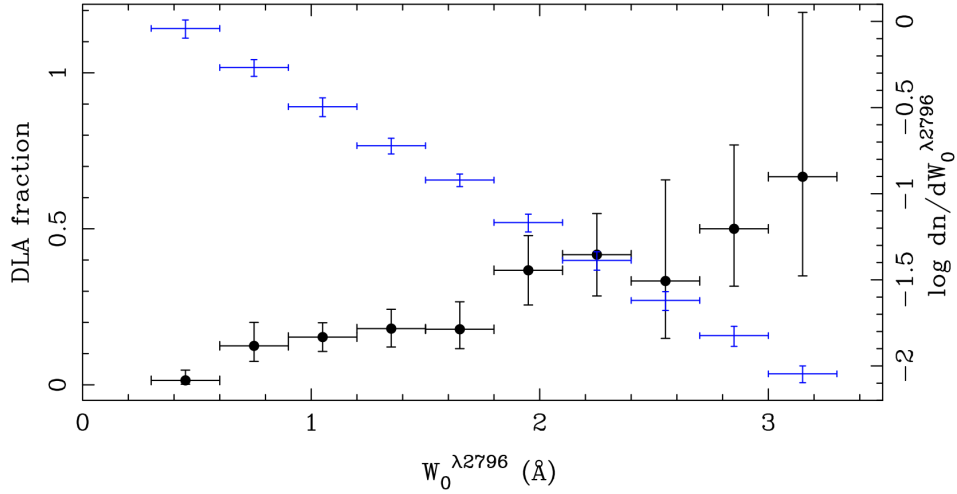


**Figure 11.** The black data points are the DLA fraction in Mg II systems as a function of  $W_0^{\lambda 2796}$  and are the same as in Figure 2. The blue points and the right vertical axis represent the cosmic  $W_0^{\lambda 2796}$  distribution of Mg II systems for  $W_0^{\lambda 2796} \geq 0.3 \text{ \AA}$  for the mean redshift of our sample,  $\langle z \rangle = 0.8$ , from NTR05.

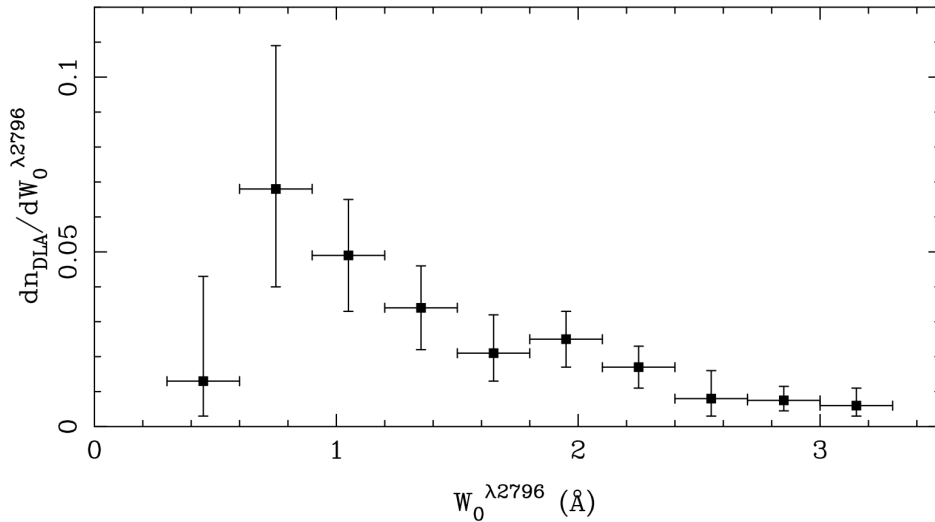


**Figure 12.** The cosmic number density of DLAs as a function of  $W_0^{\lambda 2796}$ , calculated as the product of the two distributions shown in Figure 11. Mg II systems with  $0.6 \text{ \AA} \leq W_0^{\lambda 2796} < 1.5 \text{ \AA}$  contribute 61% of the total number density of DLAs.

for DLA metallicities at  $[X/H] \sim -2$ . The reason for the metallicity-kinematics relation is far from understood (§1), but our investigation of neutral gas properties has revealed an apparent floor for both metallicity as well as velocity spread of neutral gas structures at low redshift. It is also interesting to note that studies of the incidence of  $W_0^{\lambda 2796}$  show a change in slope for the distribution of  $dn/dW_0^{\lambda 2796}$  at  $W_0^{\lambda 2796} \sim 0.3 \text{ \AA}$  (NTR05; Narayanan et al. 2007), indicating the possibility that this threshold might represent two distinct populations of absorbers.

Second, Figure 10 also shows that measurements of DLA metallicities have apparently sampled  $W_0^{\lambda 2796}$  values fairly uniformly across the range of rest equivalent widths  $0.3 \text{ \AA} \leq W_0^{\lambda 2796} \leq 3.8 \text{ \AA}$ . However, the rest equivalent distribution of Mg II  $\lambda 2796$  is a strong function of  $W_0^{\lambda 2796}$ , with

$W_0^{\lambda 2796} = 4 \text{ \AA}$  systems being nearly three orders of magnitude less common than  $W_0^{\lambda 2796} = 0.3 \text{ \AA}$  systems (NTR05). Therefore, in the end, observers studying the average cosmic metallicity need to be aware of the fact that by selecting a DLA system with a higher gas velocity spread (i.e., a higher  $W_0^{\lambda 2796}$  value) they will be tending to select a DLA with higher metallicity. Thus, an unbiased sample for a DLA metallicity study should be designed to have a relative distribution of  $W_0^{\lambda 2796}$  values that matches that of the true DLA population. But, as we have discussed, in order to increase the probability of finding DLAs, our survey methods have tended to select high  $W_0^{\lambda 2796}$  systems. We account for this when we calculate the cosmic incidence of DLAs (§3.2). Similarly, calculations of cosmic metallicity should account for this as well or they might inadvertently be using a non-representative sample.

Figures 11 and 12 illustrate this further. In Figure 11, the left vertical axis and the black solid data points are the same as in Figure 2. On the right vertical axis and as blue data points, we plot the Mg II rest equivalent distribution from NTR05, which is plotted for the mean redshift of our sample,  $\langle z \rangle = 0.8$ , and for the range of  $W_0^{\lambda 2796}$  in our sample,  $0.3 \text{ \AA} \leq W_0^{\lambda 2796} < 3.3 \text{ \AA}$ . Figure 12 shows the product of these two quantities, which gives the incidence of DLAs as a function of  $W_0^{\lambda 2796}$ ; Mg II systems with  $0.6 \text{ \AA} \leq W_0^{\lambda 2796} < 1.5 \text{ \AA}$  are seen to contribute  $\sim 61\%$  of the total number density of DLAs. Thus, when determining the mean neutral-gas cosmic metallicity of the universe, samples of DLAs should be selected according to the appropriate relative numbers of their  $W_0^{\lambda 2796}$  values (or equivalently, velocity spread values). We also point out that the two-orders-of-magnitude spread in metallicity measurements of DLAs at all redshifts is, at least in part, a manifestation of the metallicity-velocity spread relation that exists within absorber samples. That the mean metallicity of DLA absorbers evolves with redshift might then be closely linked to the redshift evolution of the Mg II rest equivalent distribution,  $dn/dW_0^{\lambda 2796}$ . However, since the  $W_0^{\lambda 2796}$ -metallicity-redshift relation is not the main purpose of this paper, we will not explore this further here.

## 5 CONCLUSIONS

We have used the Mg II selection method to perform an unbiased survey for DLA absorption line systems at  $0.11 < z < 1.65$ . The results represent an update to our previous findings reported in RTN06. In particular, three new subsamples of Mg II absorbers were investigated using UV spectroscopy to determine if they had a DLA line indicative of  $N_{\text{HI}} \geq 2 \times 10^{20} \text{ atoms cm}^{-2}$ . The previous RTN06 sample had 41 DLAs in 197 Mg II systems, and updates to this sample now include 26 DLAs in 96 Mg II systems from our HST ACS Prism Survey, three DLAs in 60 Mg II systems from our GALEX Archival Survey, and zero DLAs in 16 Mg II systems from our MMT-HST COS Survey (although two systems from this survey that did not qualify to be in our statistical sample were DLAs, §2.3). Each one of these new subsamples had a specific  $W_0^{\lambda 2796}$  rest equivalent width,  $W_0^{\lambda 2796}$ , selection criterion threshold. These thresholds had to be taken into account when deriving the updated DLA statistical results since, as described in §3.1, the probability of detecting a DLA in a Mg II system depends on  $W_0^{\lambda 2796}$  (Figure 2). In total this new, updated sample includes 70 DLAs in 369 Mg II systems with  $W_0^{\lambda 2796} \geq 0.3 \text{ \AA}$ . Analysis of this new, updated sample indicate the following:

1. The incidence of DLAs, or product of their gas cross section and their comoving number density, can be described by  $n_{\text{DLA}}(z) = (0.027 \pm 0.007)(1+z)^{(1.682 \pm 0.200)}$ . Only the results of N12 for redshifts  $2 < z < 3.5$  and our current results for  $0.11 < z < 1.65$  were used to derive this relation. It is shown in Figure 4 as the black curve. This relation appears to hold over the redshift interval  $0 < z < 5$  and is in good agreement with the 21 cm emission results reported by B12 at  $z = 0$ .

2. The cosmic mass density of neutral gas can be described by  $\Omega_{\text{DLA}}(z) = (4.77 \pm 1.60) \times 10^{-4} (1+z)^{(0.64 \pm 0.27)}$ . Once again,

only the N12 high redshift and our current low redshift results were used to derive this relation. The curve is shown in Figure 6. Given the large uncertainties in our low redshift data points, the fit should not be used to draw any conclusions regarding its extrapolated value to  $z = 0$ , although it is formally more consistent with the Z05 result.

3. The results on the HI column density distribution,  $f(N)$ , are shown in Figure 7. The best-fitting power law for our data points in the range  $20.3 \leq \log N_{\text{HI}} < 21.8$  has a power law index of  $-1.46 \pm 0.20$ . At the lowest  $N_{\text{HI}}$  values our results lie between the  $z = 0$  21 cm emission results of Z05 and B12, with the B12 results being several times lower than the Z05 results. In terms of a possible trend, the low  $N_{\text{HI}}$  tail of the DLA  $f(N)$  distribution is seen to decrease as one progresses from high redshift (N12), to low redshift (this study), to  $z = 0$  (B12), although to establish this we would need to more clearly understand why the results of Z05 and B12 disagree. At the highest  $N_{\text{HI}}$  values our results are more consistent with the  $z = 0$  21 cm emission results of B12, which are also similar to the results of N12.

Finally, in §4 we addressed the possibilities that the Mg II selection method for DLAs leads to either  $\langle N_{\text{HI}} \rangle$  values that are biased high or a metallicity bias. The results shown in Figures 8 and 9, respectively, show that both of these possibilities can be rejected with certainty in the redshift interval  $0.11 < z < 1.65$ , which is the UV DLA redshift regime. Thus, at least at  $z < 1.65$ , DLAs found through Mg II selection statistically represent the true population of DLAs. We also caution that studies of DLA metallicities should take into account the relative incidence of DLAs with respect to  $W_0^{\lambda 2796}$  (or gas velocity spread) in order to correctly measure the mean cosmic metallicity of the universe.

## ACKNOWLEDGMENTS

We thank Dan Nestor for his contributions to earlier parts of this study.

The SDSS is managed by the Astrophysical Research Consortium for the Participating Institutions. The Participating Institutions are the American Museum of Natural History, Astrophysical Institute Potsdam, University of Basel, University of Cambridge, Case Western Reserve University, University of Chicago, Drexel University, Fermilab, the Institute for Advanced Study, the Japan Participation Group, Johns Hopkins University, the Joint Institute for Nuclear Astrophysics, the Kavli Institute for Particle Astrophysics and Cosmology, the Korean Scientist Group, the Chinese Academy of Sciences (LAMOST), Los Alamos National Laboratory, the Max-Planck-Institute for Astronomy (MPIA), the Max-Planck-Institute for Astrophysics (MPA), New Mexico State University, Ohio State University, University of Pittsburgh, University of Portsmouth, Princeton University, the United States Naval Observatory, and the University of Washington.

## REFERENCES

Bahcall et al. 1993, ApJS, 87, 1

- Battisti, A. J., Meiring, J. D., Tripp, T. M., Prochaska, J. X., Werk, J. K., Jenkins, E. B., Lehner, N., Tumlinson, J., Thom, C. 2012, *ApJ*, 744, 93
- Bordoloi et al. 2014, *ApJ*, 784, 108
- Bouché et al. 2012, *MNRAS*, 426, 801
- Braun, R. 2012, *ApJ*, 749, 87 (B12)
- Crighton, N. H. M. et al. 2015, *MNRAS*, 452, 217
- Delhaize, J., Meyer, M. J., Staveley-Smith, L., Boyle, B. J. 2013, *MNRAS*, 433, 1398
- Dessauges-Zavadsky, M., Ellison, S. L., Murphy, M. T. 2009, *MNRAS*, 396, L61
- Ellison, S. L., York, B. A., Pettini, M., Kanekar, N. 2008, *MNRAS*, 388, 1349
- Ellison, S. L., Kanekar, N., Prochaska, J. X., Momjian, E., Worseck, G. 2012, *MNRAS*, 424, 293
- Hoppmann, L., Staveley-Smith, L., Freudling, W., Zwaan, M. A., Minchin, R. F., Calabretta, M. R. 2015, 452, 3726
- Jorgenson, R. A., Wolfe, A. M., Prochaska, J. X., Lu, L., Howk, J. C., Cooke, J., Gawiser, E., Gelino, D. M. 2006, *ApJ*, 646, 730
- Jorgenson, R. A., Murphy, M. T., Thompson, R. 2013, *MNRAS*, 435, 482
- Kanekar, N., Prochaska, J. X., Ellison, S. L., Chengalur, J. N. 2009, *MNRAS*, 396, 385
- Kulkarni, V. P., Fall, M. S., Lauroesch, J. T., York, D. G., Welty, D. E., Khare, P., Truran, J. W. 2005, *ApJ*, 618, 68
- Kulkarni, V. P., Khare P., Péroux C., York D. G., Lauroesch J. T., Meiring J. D. 2007, *ApJ*, 661, 88
- Kulkarni, V. P., Khare, P., Debopam, S., Meiring, J., York, D. G., Péroux, C., Lauroesch, J. T. 2010, *NewA*, 15, 735
- Kulkarni, V. P., Som, D., Morrison, S., Péroux, C., Quiret, S., York, D. G. 2015, *ApJ*, 815, 24
- Lacy, M., Becker, R. H., Storrie-Lombardi, L. J., Gregg, M. D., Urrutia, T., & White, R. L. 2003, *AJ*, 126, 2230
- Lah, P. et al. 2007, *MNRAS*, 376, 1357
- Lanzetta, K. M., Wolfe, A. M., Turnshek, D. A., Lu, L., McMahon, R. G., Hazard, C. 1991, *ApJS*, 77, 1
- Ledoux, C., Petitjean, P., Fynbo, J. P. U., Møller, P., Srianand, R. 2006, *A&A*, 457, 71
- Lu, L., Wolfe, A. M., Turnshek, D. A., Lanzetta, K. M. 1993, *ApJS*, 84, 1
- Lu, L., Wolfe, A. M. 1994, *AJ*, 108, 44
- Martin, A. M., Papastergis, E., Giovanelli, R., Haynes, M. P., Springob, C. M., Stierwalt, S. 2010, *ApJ*, 723, 1359
- Matejek, M. S., Simcoe, R. A., Cooksey, K., L., Seyffert, E. N. 2013, *ApJ*, 764, 9
- Meiring, J. D. et al. 2006, *MNRAS*, 370, 43
- Meiring, J. D. et al. 2011, *ApJ*, 732, 35
- Møller, P., Fynbo, J. P. U., Ledoux, C., Nilsson, K. K. 2013, *MNRAS*, 430, 2680
- Monier, E. M., Turnshek, D. A., Rao, S. M., Weyant, A. 2009, *AJ*, 138, 1609
- Morrissey, P. et al. 2007, *ApJS*, 173, 682
- Murphy, M. T., Curran S. J., Webb, J. K., Ménager, H., Zych, B. J. 2007, *MNRAS*, 376, 673
- Narayanan, A., Misawa, T., Charlton, J. C., Kim, T.-S. 2007, *ApJ*, 660, 1093
- Neeleman, M., Prochaska, J. X., Ribaldo, J., Lehner, N., Howk, J. C., Rafelski, M., Kanekar, N. 2016, *ApJ*, 818, 113
- Nestor, D. B., Rao, S. M., Turnshek, D. A., vanden Berk, D. 2003, *ApJ*, 595, L5
- Nestor, D. B. 2004, Ph.D. Thesis, U. Pittsburgh
- Nestor, D. B., Turnshek, D. A., Rao, S. M. 2005, *ApJ*, 628, 637 (NTR05)
- Nestor, D. B., Turnshek, D. A., Rao, S. M. 2006, *ApJ*, 643, 75
- Nestor, D. B., Pettini, M., Hewett, P. C., Rao, S., Wild, V. 2008, *MNRAS*, 390, 1670
- Noterdaeme, P., Petitjean, P., Ledoux, C., Srianand, R. 2009, *A&A*, 505, 1087
- Noterdaeme, P., et al. 2012, *A&A*, 547, L1 (N12)
- Péroux, C., McMahon, R. G., Storrie-Lombardi, L., Irwin, M. J. 2003, *MNRAS*, 346, 1103
- Prochaska, J. X., Herbert-Fort, S. 2004, *PASP*, 116, 622
- Prochaska, J. X., Herber-Fort, S., Wolfe, A. M. 2005, *ApJ*, 635, 123
- Prochaska, J. X., Wolfe, A. M. 2009, *ApJ*, 696, 1543
- Quider, A. M., Nestor, D. B., Turnshek, D. A., Rao, S. M., Monier, E. M., Weyant, A. J., Busche, J. R. 2011, *AJ*, 141, 137
- Quiret, S., PÁlroux, C., Zafar, T., Kulkarni, V. P., Jenkins, E. B., Milliard, B., Rahmani, H., Popping, A., Rao, S. M., Turnshek, D. A., Monier, E. M. 2016, *MNRAS*, 458, 4074
- Rafelski, M., Wolfe, A. M., Prochaska, J. X., Neeleman, M., Mendez, A. 2012, *ApJ*, 755, 89
- Rao, S., Turnshek, D. A., Briggs, F. H. 1995, *ApJ*, 449, 488
- Rao, S. M., Turnshek, D. A. 2000, *ApJS*, 130, 1
- Rao, S. M., Nestor, D. B., Turnshek, D. A., Lane, W. M., Monier, E. M., Bergeron, J. 2003, *ApJ*, 595, 94
- Rao, S. M., Prochaska, J. X., Howk, C. J., & Wolfe, A. M. 2005, *AJ*, 129, 9
- Rao, S. M., Turnshek, D. A., Nestor, D. B. 2006, *ApJ*, 636, 610 (RTN06)
- Rao, S., Belfort-Mihalyi, M., Turnshek, D., Monier, E., Nestor, D., Quider, A. 2011, *MNRAS*, 416, 1215
- Rhee, J., Zwaan, M. A., Briggs, F. H., Chengalur, J. N., Lah, P., Oosterloo, T., van der Hulst, T. 2013, *MNRAS*, 435, 2693
- Sánchez-Ramírez, R. et al. 2016, *MNRAS*, 456, 4488
- Steidel, C. C., Sargent, W. L. W. 1992, *ApJS*, 80, 1
- Seyffert, E. N., Cooksey, K. L., Simcoe, R. A., O'Meara, J. M., Kao, M. M., Prochaska, J. X. 2013, *ApJ*, 779, 161
- Som, D., Kulkarni, V. P., Meiring, J., York, D. G., Péroux, C., Lauroesch, J. T., Aller, M. C., Khare, P. 2015, *ApJ*, 806, 25
- Storrie-Lombardi, L., Wolfe, A. M. 2000, *ApJ*, 543, 552
- Tumlinson, J. et al. 2013, *ApJ*, 777, 59
- Turnshek, D. A., Wolfe, A. M., Lanzetta, K. M., Briggs, F. H., Cohen, R. D., Foltz, C. B., Smith, H. E., Wilkes, B. J. 1989, *ApJ*, 344, 567
- Turnshek, D. A., Rao, S. M., Nestor, D. B., Belfort-Mihalyi, M., Quider, A. M. 2005, *IAU Symp* 235, 440, arXiv:astro-ph/0506701
- Turnshek, D. A., Monier, E. M., Rao, S. M., Hamilton, T. S., Sardane, G. M., Held, R. 2015, *MNRAS*, 449, 1536
- Wolfe, A. M., Turnshek, D. A., Smith, H. E., Cohen, R. D. 1986, *ApJS*, 61, 249
- Wolfe, A. M., Gawiser, E., Prochaska, J. X. 2005, *ARA&A*, 43, 861
- Zafar, T., Péroux, C., Popping, A., Milliard, B., Deharveng, J.-M., Frank, S. 2013, *A&A*, 556, A141
- Zafar, T., Popping, A., Péroux, C. 2013, *A&A*, 556, A140
- Zhu, G., Menard, B. 2013, *ApJ*, 770, 130
- Zwaan, M. A., van der Hulst, J. M., Briggs, F. H., Verheijen, M. A. W., Ryan-Webber, E. V. 2005, *MNRAS*, 364, 1467 (Z05)

This paper has been typeset from a  $\text{\TeX}/\text{\LaTeX}$  file prepared by the author.